Modeling Plasma Virus Concentration and CD4+ T Cell Kinetics during Primary HIV Infection

Max A. Stafford
Yunzhen Cao
David D. Ho
Lawrence Corey
Crystal L. Mackall

SFI WORKING PAPER: 1999-05-036

SANTA FE INSTITUTE

Modeling Plasma Virus Concentration and CD4+ T Cell Kinetics during Primary HIV Infection

MAX A. STAFFORD[1,2], YUNZHEN CAO[3], DAVID D. HO[3], LAWRENCE COREY[4], AND ALAN S. PERELSON[5]

[1] *Santa Fe Institute,* 1399 *Hyde Park Rd., Santa Fe, NM 87501, U.S.A*

[2.] *Computing and Mathematical Sciences Department, Texas A&M University-Corpus Christi, 6300 Ocean Drive, Corpus Christi, TX 78412, U.S.A.*

[3]*Aaron Diamond AIDS Research Center, The Rockefeller University, 455 First Avenue, New York, NY 10016, U.S.A*

[4] *Hutchison Cancer Research Center, Program in Infectious Disease, 1100 Fairview Avenue North, Seattle, WA 98109, U.S.A*

[5] *Theoretical Biology and Biophysics, Theoretical Division, Los Alamos National Laboratory, Los Alamos, NM 87545, U.S.A.*

During primary HIV infection the viral load in plasma increases, reaches a peak, and then declines. Phillips has suggested that the decline is due to a limitation in the number of cells susceptible to HIV infection, while other authors have suggested that the decline in viremia is due to an immune response. Here we address this issue by developing models of primary HIV-1 infection, which include T cell kinetics, and by comparing predictions from these models with data from nine, anti-retroviral drug-naive infected patients. Applying nonlinear least squares estimation, we find that relatively small variations in parameters are capable of mimicking the highly diverse patterns found in patient viral load data. This approach yields an estimate of two days for the lifespan of productively infected cells during primary infection, a value that is consistent with results obtained by drug perturbation experiments. We find that all patient data sets considered are consistent with a target-cell limited model from the time of initial infection until shortly after the peak in viremia, but some data sets are not consistent after the peak value with the assumptions of such a model. We illustrate that two possible immune response mechanisms, cytotoxic T lymphocyte destruction of infected target cells and cytokine suppression of viral replication, could account for declines in viral load data not predicted by the original target-cell limited model. We conclude that some additional process, perhaps mediated by CD8+ T cells, is important in at least some patients.

1. Introduction

1.1 Background

During primary HIV infection, viral load increases sharply during the first few weeks after infection and then declines rapidly, ultimately reaching a quasi-steady state or set point level (Daar *et al.*, 1991; Schacker *et al*., 1996; Kahn & Walker, 1998). Phillips (1996) suggested that the sharp decline in virus concentration might be the result of target-cell limitation, *i.e.*, the running out of new cells for the virus to infect. Phillips demonstrated that simulations of a simple model based on this assumption produce a 'spike' in virus concentration qualitatively similar to that observed in patients. Another explanation for the viral decline is that an anti-viral immune response, for example, the cytotoxic T cell response (Koup *et al.*, 1994; Rinaldo *et al*., 1995; Riviere *et al*., 1995; Pantaleo *et al*., 1997; Matano *et al*., 1998; Schmitz *et al*., 1999), brings the viral load in check. The question of whether the drop in viral load is primarily the result of an anti-viral immune response or target-cell limitation has yet to be answered satisfactorily.

This issue is addressed here by developing dynamic models of the events that occur during the first 100 days following primary HIV-1 infection, and comparing model predictions with clinical data. Models of primary infection have also been developed by Phillips (1996), Nowak *et al.* (1997a) and Murray *et al.* (1998). In addition, numerous models of AIDS pathogenesis have been proposed to capture the progression to AIDS following the initial viral spike (Reibnegger *et al.*, 1989; Hraba *et al.*, 1990; Nowak *et al.*, 1990; McLean and Kirkwood, 1990; Nowak *et al.*, 1991; McLean *et al.*, 1992, Perelson *et al.*, 1993; Essunger *et al.*, 1994; Schenzle *et al.*, 1994; Kirschner *et al.*, 1998; Stilianakis *et al.*, 1997). A comprehensive model—one capable of predicting the spike, the asymptomatic phase, and progression to AIDS—is ultimately desired, but much can be learned by studying the early events. The characteristic spike in viral load provides a distinctive landmark against which differential equation models can be validated.

Figure 1 depicts the virus concentration in a representative HIV-positive patient studied at the Aaron Diamond AIDS Research Center. A viral spike similar to the one shown in Fig. 1 occurs in all nine patient data sets that we investigate. Our goal is to develop a model that can account for the initial rise, subsequent fall, and stabilization of the virus concentration at a set-point level.

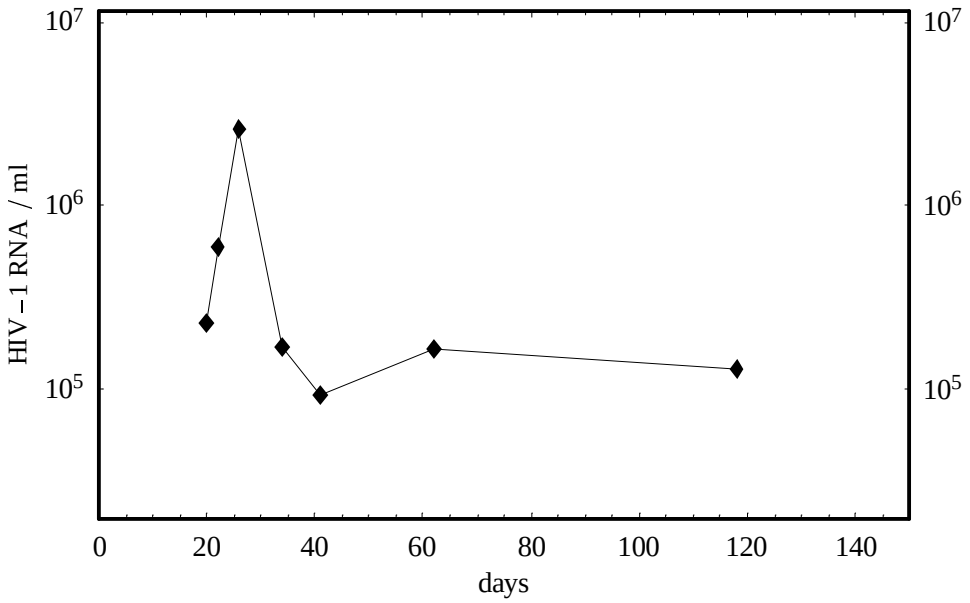

Figure 1. Representative virus concentration time history. The time of initial infection is unknown so the point labeled *t=0* is arbitrary.

1.2 Overview

In the following section we derive a simple CD4+ T cell population dynamic model that includes a thymus, and activated and resting subsets of peripheral blood CD4+ T cells. We then expand this model to include infected resting and infected activated CD4+ T cells and virus density. Simplifications of this full model lead to a simple three-equation model for target-cell limited viral infection that has been used in other studies (Wei *et al*., 1995; Perelson *et al*., 1996; Nowak *et al*., 1997a).

In Section 3, nonlinear least squares estimation is applied to the three-equation model to determine parameters associated with each of the nine patient viral load data sets. We find that modest variations in the parameters of the model are capable of mimicking the wide patient-to-patient variation in the rise and initial decline in viremia. Following the initial decline, however, we find viral load in many patients falls below the quasi-steady state viral load predicted by the simplified model. We document this pattern in the beginning of Section 4 , then explore two widely-discussed methods of immune control that could account for the discrepancies—increased rate of killing of productively infected cells by cytotoxic T lymphocytes (CTLs) and suppression of viral production by cellular antiviral factors (CAFs).

In Section 5 we show that simplifications made in deriving the simple model used for parameter estimation were justified. We also illustrate that the full model gives reasonable predictions for changes in CD4+ T cell subsets during primary infection and in the early asymptomatic stage. Observations and summary comments are given in Sections 6 and 7, respectively.

2. Assumptions and Model Development

2.1 Model of CD4+ T Cell Kinetics

Pluripotent stem cells produced in the bone marrow migrate to the thymus where they mature into fully functional T cells (Paul, 1993). The mature T cells that emerge generally have either CD4 or CD8 molecules on their surface. Here we restrict our attention to CD4+ T cell dynamics, and use the term precursor to refer to the cells in the thymus destined to become CD4+ T lymphocytes. We describe CD4+ T cells as either quiescent or activated.

The dynamics of the precursor, *P*, quiescent CD4+ T cell, *Q*, and activated CD4+ T cell, *T*, populations in a healthy individual (non-HIV infected) are modeled by the following equations:

$$\begin{aligned}
\frac{dP(t)}{dt} &= s + rP\left(1 - \frac{P}{P_{\max}}\right) - \tilde{b}P \\
\frac{dQ(t)}{dt} &= bP - aQ\left(1 - \frac{Q+T}{T_{\max}}\right) - \mu_Q Q + 2fpT \\
\frac{dT(t)}{dt} &= aQ\left(1 - \frac{Q+T}{T_{\max}}\right) + (1-2f)pT - \mu_T T
\end{aligned} \tag{2.1}$$

In the precursor equation, *s* is the rate of influx of stem cells from bone marrow, $\tilde{b}$ and *b* represent rate constants for the export of precursors from the thymus into the quiescent CD4+ T cell compartment but given in different units, *r* is the net maximum growth rate of precursors, and P_{max} is the precursor population size at which proliferation shuts off. This type of growth term represents self-limiting cell proliferation and the rate of loss of precursors by death is incorporated into the net maximum growth rate *r*. We express *Q* and *T* in units of cells/mm^3, and thus *b* is the number of cells that enter a mm^3 of blood per unit time.

The precursor equation was derived by scaling the following differential equation for total number of CD4+ T cell precursors in the thymus,

$$\frac{d\mathcal{P}(t)}{dt} = s + r\mathcal{P}\left(1 - \frac{\mathcal{P}}{\mathcal{P}_{\max}}\right) - \tilde{b}\mathcal{P},$$

such that $P=\sigma\mathcal{P}$. Letting σ be the reciprocal of the scaling factor used to extrapolate from peripheral blood lymphocyte density to whole body ($50\times5\times10^6$), i.e., $\sigma=4\times10^{-9}$, allows the coefficients *b* and $\tilde{b}$ to have the same numerical value and differ only in units. Assuming there are 5×10^{10} thymocytes in an adult thymus (Kirschner *et al*., 1998), and that half of these are CD4+ T cell precursors, our scaling yields a steady state dimensionless value of 100 for *P*.

The first term in the quiescent cell equation represents the rate of influx of mature CD4+ T cells from the thymus. Quiescent cells are assumed to become activated at a rate given by a logistic law with maximum rate of activation per cell, a, and maximum population size, T_{max}, and to be lost by death at per capita rate μ_Q. Quiescent cells are also generated by division of activated cells as described below.

Activated cells, T, are generated by activation of resting cells or division of activated cells, and are lost due to death or apoptosis at per capita rate μ_T. Cells leave the activated pool at a rate proportional to T, $-pT$. A fraction of these, f, are assumed to divide and become quiescent cells while the remainder, $(1-f)$, divide and return to the activated pool. These rates combine, $-pT + 2(1-f)pT = (1-2f)pT$, yielding the term in the rate equation that accounts for change of activated cells. Note that this term represents a net loss from the activated pool if $f > 0.5$ and a net gain to the activated pool if $f < 0.5$. The progeny that leave the activated pool account for the $2fpT$ term in the equation for Q.

There are two significant features of this model. First, loss of thymic output, such as in a thymectomy, leads to a positive steady state value for the total CD4+ T cell density for parameter values used herein. A second feature is that it distinguishes between resting and activated cells. The model is similar to one proposed by Stilianikis *et al*. (1997). Other models that distinguish resting and activated cells have also been developed (McLean and Kirkwood, 1990; McLean and Nowak, 1992; Essunger and Perelson, 1994).

Both resting and activated T cells are lost by natural death. The symbols μ_Q and μ_T denote the natural death rate constants for resting and activated cells, respectively. These constants are not well known and we use a nominal value of 0.005 day^{-1} for μ_Q and 0.2 day^{-1} for μ_T. The higher value for μ_T reflects the increased likelihood of apoptosis following activation of a CD4+ T cell (Abbas, 1996).

Combining the steady state value of precursors of 100 and an assumed value of 0.15 /day for the export rate constant $\tilde{b}$ results in a thymus source of 1.5 cells/mm^3-day or, for a person with 5 liters of blood, at a total rate of 7.5×10^6 /day. Since only 2% of CD4+ T cells are in the blood, this corresponds to a total production rate of 3.75×10^8 /day, which implies it would take 670 days to totally reconstitute an empty immune system to the standard value for an adult of 2.5×10^{11} CD4+ T cells. Such a slow reconstitution is consistent with measurements made by Mackall *et al.* (1995). In a study of multiple sclerosis patients, a similar shallow rate of recovery in CD4+ T cell density was noted in the first six months following depletion of CD4+ T cells by an anti-CD4 monoclonal antibody (Lindsey *et al*., 1994).

Steady state values for Q and T of 990 cells/mm^3 and 10 cells/mm^3, respectively, were selected to correspond to 1% activation in peripheral blood (Sachsenberg *et a*l., 1998). Proliferation and death rate constants for activated cells, and the parameter f are such that the net proliferation rate constant, $(1-2f)p$, is less than the death rate constant, μ_T, as observed in SIV-infected monkeys (Mohri *et al*., 1998). A complete list of the parameter values for the model is given in Table 1.

The model and parameter values are consistent with a patient data set from a recent investigation of thymopoiesis (Mackall *et al.*, 1995). In that study, measurements were obtained following cessation of intensive chemotherapy treatments administered to a patient suffering from an inoperable brain tumor. The filled circles in Fig. 2 represent total CD4+ T cell counts for this patient. It was assumed that thymocytes were depleted to the same degree as the peripheral CD4+ T cell level (*i.e.*, to 1% of their original value).

Parameter	*Description*	*Value*
P_{max}	max precursor population	142.7
T_{max}	max CD4+ T cell density	1500 cells/μl
s	bone marrow source rate	0.004 d^{-1}
f	fraction returning to quiescent cells	0.324
μ_Q	death rate, resting cells	0.005 d^{-1}
μ_T	death rate, activated cells	0.2 d^{-1}
r	max growth rate of precursors	0.05 d^{-1}
$\tilde{b}$	export rate of precursors	0.015 d^{-1}
a	activation rate constant	0.00025 d^{-1}
p	proliferation rate constant	0.545 d^{-1}

Table 1. Parameter values used in the CD4+ T cell kinetic model. Values for P_{max}, f, and p were derived by imposing equilibrium values of 100, 990 cells/μl, and 10 cells/μl on P, Q, and T, respectively. Due to our scaling of the precursor equation, b and $\tilde{b}$ have the same numerical value.

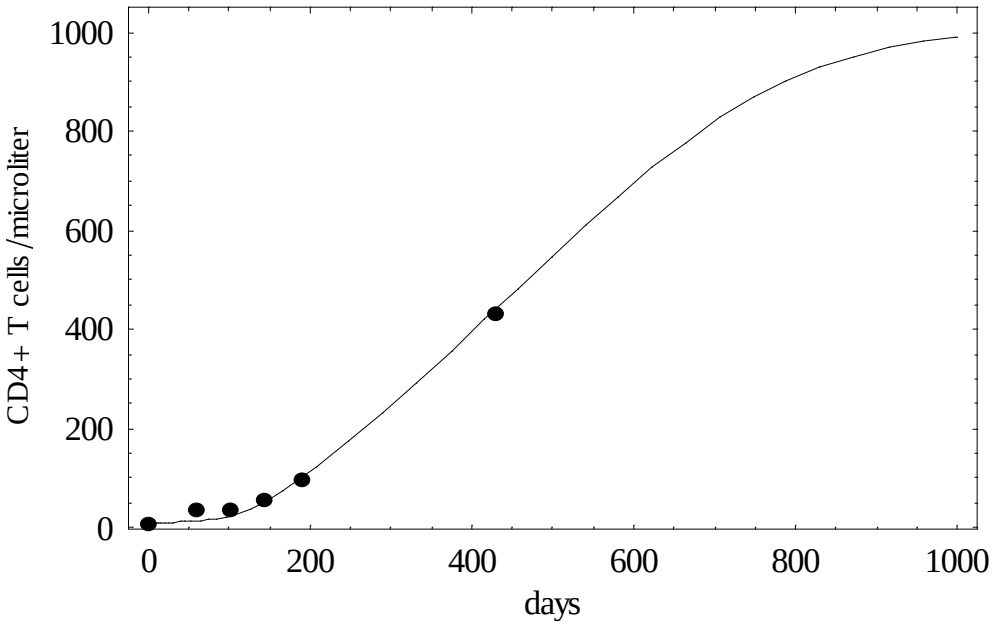

Figure 2. Comparison of one patient's re-scaled CD4+ T cell density during recovery following chemotherapy (●) and simulation results from the infection-free model. Data taken from Mackall *et al.* (1995).

The above model, with parameter values given in Table 1, produced the result shown by the curve in Fig. 2. These results show that the model and parameter values are consistent with the dynamics observed by Mackall *et al.* (1995) in one adult patient.

However, these parameter values are not unique and different sets of parameters can be found which give nearly identical results when fitted to the data in Mackall *et al.* (1995). Thus, the parameter values in Table 1 should be viewed as a working set of parameter values that may be subject to change as further experimental measurements become available.

2.2 Infected Cell Model

HIV-1 infects lymphocytes bearing the CD4 molecule (Fauci, 1988). Thus, to model HIV-1 infected patients we add equations to the infection-free model to account for infected quiescent T cells (Q^*), infected activated T cells (T^*), and the free virion density (V). The following system is proposed:

$$
\begin{aligned}
\frac{dP(t)}{dt} &= s + rP\left(1 - \frac{P}{P_{\max}}\right) - \tilde{b}P \\
\frac{dQ(t)}{dt} &= bP + 2fpT - aQ\left(1 - \frac{T_{tot}}{T_{\max}}\right) - \mu_Q Q \\
\frac{dQ^*(t)}{dt} &= \phi kTV - \mu_L Q^* - a_L Q^* \\
\frac{dT(t)}{dt} &= aQ\left(1 - \frac{T_{tot}}{T_{\max}}\right) + (1-2f)pT - \mu_T T - kTV \\
\frac{dT^*(t)}{dt} &= (1-\phi)kTV + a_L Q^* - \delta T^* \\
\frac{dV(t)}{dt} &= \pi T^* - kTV - cV \\
T_{tot} &= Q + Q^* + T + T^*
\end{aligned}
\tag{2.2}
$$

Although it is possible for HIV to enter a resting cell, direct infection of resting cells is very inefficient due either to lack of full reverse transcription of viral RNA (Zack *et al.*, 1992) or lack of integration of the reverse transcribed DNA into the host cell's DNA (Stevenson *et al.*, 1990). Here we only consider the primary targets of infection, activated CD4+ T cells (Schnittman *et al.*, 1990). We assume that activated cells, T, become infected with rate constant k, and that a fraction ϕ of such cells revert to rest during the infection process generating resting infected cells, Q^*. The remaining fraction, 1- ϕ, of infection events are assumed to generate productively infected cells, T^*, which are

assumed to die with loss rate constant δ. If some productively infected cells revert to rest, they will generate resting infected cells Q^* (Chun *et al.*, 1997).

We assume that virus is produced from infected activated T cells at rate π per cell, is lost by infecting activated cells, and is otherwise cleared with rate constant *c*. We assume infected quiescent cells are latently infected and do not produce virus.

2.3 A Simplified Infected Cell Model

Some simplifying assumptions can be applied to reduce the full model to one involving only activated cells, infected activated cells, and virus concentration. First, we assume the thymus does not shut down immediately from infection so that the supply of quiescent cells, *bP*, remains constant. Over a relatively short period of time, say 100 days or less, we also treat the uninfected and infected quiescent cell population as essentially constant. This simplification is due to the long life span and low activation constant associated with quiescent cells. We assume the majority of newly infected activated cells remain activated and become productively infected and thus, we set ϕ to 0. Finally, we neglect the loss term from the virus concentration rate equation due to binding with T cells, *-kTV*, since this term is typically small compared with the clearance term. These simplifications lead to the following initial value problem:

$$\begin{aligned} \frac{dT(t)}{dt} &= \lambda - dT - kTV, \qquad T(0) = T_0 \\ \frac{dT^*(t)}{dt} &= kTV - \delta T^*, \qquad T^*(0) = T_0^* \\ \frac{dV(t)}{dt} &= \pi T^* - cV, \qquad V(0) = V_0 \end{aligned} \tag{2.3}$$

We have replaced the slowly varying source term from quiescent cells entering activation, $aQ\left(1-\frac{T_{tot}}{T_{\max}}\right)$, with a constant influx, λ. The term *-dT* replaces the two linear terms in the full model, *(1-2f)pT - μ_TT*, and can be thought of as a net rate of loss of activated cells from the population. Uninfected activated cells are also lost due to infection with HIV, which is represented by the term *-kTV* as in the full model. The infected cells are supplied by the loss from the target- cell pool and die at a rate proportional to their number density with constant of proportionality δ. New virions are produced by infected cells at the rate πT^* and virions are lost at a rate proportional to the virus concentration with constant of proportionality *c*.

3. Parameter Estimation Using the Simplified Model

3.1 Patient Data

Virus concentration measurements in peripheral blood from nine patients (Table 2) was obtained from two labs and used in parameter estimation. Data for patients 1 and 2 were from a University of Washington study (Schacker *et al*., 1996), and data for patients 3 through 9 were provided by the Aaron Diamond AIDS Research Center.

Specimens were taken only after patients presented with acute infection symptoms, so baseline values of CD4+ T cell density and viral load are not available. Except for one patient, the time between initial infection and the time of the first data point is unknown and must be estimated. The exact date of initial HIV-1 infection is known for patient 9 (Borrow *et al*., 1997; Clark *et al*., 1991). Values of time reported by Borrow *et al*., begin 15 days following onset of symptoms, which according to the patient, and corroborated by his sexual partner, was 20 days following initial exposure. Consequently, the data in Table 2 for patient 9, when translated forward 35 days reflect the actual rather than the estimated time following initial infection. For patients 1 and 2 the times in Table 2 are measured from onset of symptoms, while for patients 3-8 they are taken from first date of data collection.

pt1	pt2	pt3	pt4	pt5	pt6	pt7	pt8	pt9
22, 27.2	3, 469.8	0, 766.8	0, 153.0	0, 228.2	0, 939.26	0, 1350.6	0, 2217.7	0, 216.4
43, 210	11, 1600	7, 947.6	5, 284.0	2, 599.2	3, 1485.0	4, 2398.6	4, 2427.9	5, 355.2
78, 85.9	15, 42.8	9, 706.2	6, 216.0	6, 2617.4	8, 701.6	9, 337.2	7, 2200.4	8, 355.4
106, 81.1	43, 41.7	15, 14.4	14, 143.0	14, 169.6	10, 564.0	12, 340.6	11, 1134.3	12, 146.8
———	———	29, 2.3	21, 30.2	21, 93.7	15, 106.5	16, 202.3	14, 705.9	19, 100.9
146, 46.2	71, 12.22	36, 1.1	32, 6.4	42, 165.6	17, 11.2	19, 169.7	18, 447.8	29, 34.7
183, 60.1	99, 14.17	50, 1.0	39, 4.1	———	22, 87.3	23, 141.4	21, 412.7	———
230, 82.8	129, 18.2	57, 1.8	46, 5.85	98, 127.0	24, 20.6	26, 56.48	26, 302.1	57, 11.4
268, 103.	197, 70.8	64, 2.1		203, 65.9	29, 14.78	30, 182.75	29, 118.8	121, 17.3
358, 72.1	255, 16.3			329, 144.7	36, 27.5	50, 267.0	33, 248.8	197, 90.1
435, 79.4	330, 81.2				———	60, 182.7	36, 173.6	280, 68.2
489, 70.4					64, 6.32	———	40, 131.3	376, 55.3
519, 207.					273, 2.27	213, 186.3	49, 259.1	525, 94.5
534, 42.6					288, 5.64	551, 89.4	———	604, 34.4
584, 10.8					347, 14.55		56, 132.24	645, 61.7
610, 54.2					430, 13.6		63, 103.2	757, 55.9
687, 22.3					478, 13.1		75, 117.1	776, 52.7
778, 40.8							547, 5.62	
							659, 24.24	

Table 2. Virus concentration data. Data points are presented as ordered pairs with first number in each entry representing a relative time in days and the second number in each entry the virus concentration in thousands of HIV-1 RNA copies/ml. A horizontal line in a column indicates only the data points above the line were used in parameter estimation. All points were used if there is no horizontal line. Patient 9 times are from 35 days following initial infection (Borrow *et al*., 1997). Patients (pt) 1 and 2 are patient numbers 1019 and 1113 from University of Washington study. Patients 3 through 9 are JSW-DAAR, CMO-DAAR, HOBR-SHAW, SUMA-SHAW, BORI-SHAW, INME-SHAW, and WEAU-SHAW from Aaron Diamond AIDS Research Center, respectively.

3.2 Nonlinear Least Squares Parameter Estimation

The simplified model (Eq. 2.3) is repeated here for convenience:

$$\begin{aligned}
\frac{dT(t)}{dt} &= \lambda - dT - kTV, \qquad T(0) = T_0 \\
\frac{dT^*(t)}{dt} &= kTV - \delta T^*, \qquad T^*(0) = T_0^* \qquad (2.3) \\
\frac{dV(t)}{dt} &= \pi T^* - cV, \qquad V(0) = V_0
\end{aligned}$$

Assuming that target cells are proliferating cells, we fix the density of target cells before infection, T_0, at 1% of the CD4+ T cell density in peripheral blood. This value is based on studies using the nuclear antigen Ki-67 (Sachsenberg *et al*., 1998) which found the percentage of proliferating CD4+ T cells in the peripheral blood of healthy controls to be 1.1± 0.6%. We assume there are no infected cells initially, so T_0^* is set to 0. We take the initial viral load, V_0, to be 10^{-6} virions/ml to represent the presence of a small number of virions present following primary infection. The exact value for V_0 is not critical since numerically it was found that varying V_0 over two orders of magnitude resulted in nearly identical virus concentration graphs except for a difference of less than four days in the predicted time to peak. Thus, V_0 and the estimated translation time of the data, τ, will play off against each other. Before infection, we assume proliferating CD4+ T cells are at equilibrium, *i.e.*, $\lambda = d\,T_0$. Hence, we need not estimate λ separately. We also accept the estimate from earlier studies (Perelson *et al.*, 1996) of the clearance rate constant, c = 3 day^{-1}, although higher values may also be reasonable (Mittler *et al*., 1998). We show in Appendix 1 that the behavior of the model depends on certain parameter products and ratios. Thus, for example, choosing a higher value of c will cause us to estimate a higher value of π. In the parameter range of interest the model's behavior is only sensitive to the value of π/c. Similarly, choosing a different initial level of activated cells, T_0, can be compensated for by changes in π.

With assumed values for T_0 , T_0^*, V_0, and c, we now estimate the remaining five parameters, d, k, δ, π and τ, for each patient, by minimizing the objective function

$$J(\theta) = \sum_{i=1}^{n} \left(\log V(t_i) - \log \hat{V}(t_i) \right)^2 \quad ,$$

where n represents the number of data points selected to estimate the vector of parameters, $\theta = [\, d, k, \delta, \pi, \tau]^T$, $V(t_i)$ represents the simulated value of virus concentration at time t_i, and $\hat{V}(t_i)$ represents the data value at time t_i with all times in the data set having been shifted by τ.

Differences in logarithms, as opposed to differences in actual values, are used in forming the objective function to accommodate the large differences between the peak values and quasi-steady state values after the peak. This approach minimizes the sums of the squared logarithms of ratios of data values to simulation values and, hence, weights ratios of small data values equally with those of large ones. Using actual values resulted in a good fit of the peak itself, but in some cases this approach gave unrealistic values for the parameters and poor agreement during the times following the peak.

The procedure for estimating the time shift, τ, for all patients other than patient 9 (whose shift is known precisely), is described in Appendix 2. Sensitivity curves obtained using different values of τ and δ provide estimates of τ, but unfortunately in some cases the estimate is not sharp. The curves do, however, demonstrate that different values for the time shift can significantly alter the estimated values of all parameters.

Table 3 summarizes the parameter estimates for d, k, δ, π, and τ, for patients 3 through 9. Figures 3 through 6 depict simulations of the simplified model (Eq. 2.3) compared with the data points for these patients. The first three figures show patient data sets that were paired because they were similar in peak values and in depths of decline in viral load following the peak. Figure 6 depicts only patient 8 data versus simulation results as this data set was unusual in two aspects—there were many, regularly spaced data points, and the decline from the peak value was atypically slow.

Patient	d	k	δ	π	τ
3	0.00899	0.000468	0.51	1060.	27.
4	0.0107	0.00185	0.258	134.	44.
5	0.0214	0.000459	0.473	1050.	25.
6	0.017	0.000469	0.5	1050.	27.
7	0.0137	0.000884	0.31	836.	16.
8	0.0112	0.000402	0.19	929.	29.
9	0.00392	0.00255	0.122	101.	35.
Mean	0.0124	0.00101	0.338	737.	29.
Sample SD	0.00565	0.000851	0.158	431.	8.7

Table 3. Estimated parameter values for patients 3 through 9. Due to dependencies among parameters in the model (discussed in Appendix 1) and an inability to estimate the time shift precisely in some patients (discussed in Appendix 2), we present these estimated values only to summarize our findings. The time unit for all parameters is days. The parameter k has units of $\mu l/virion\text{-}day$.

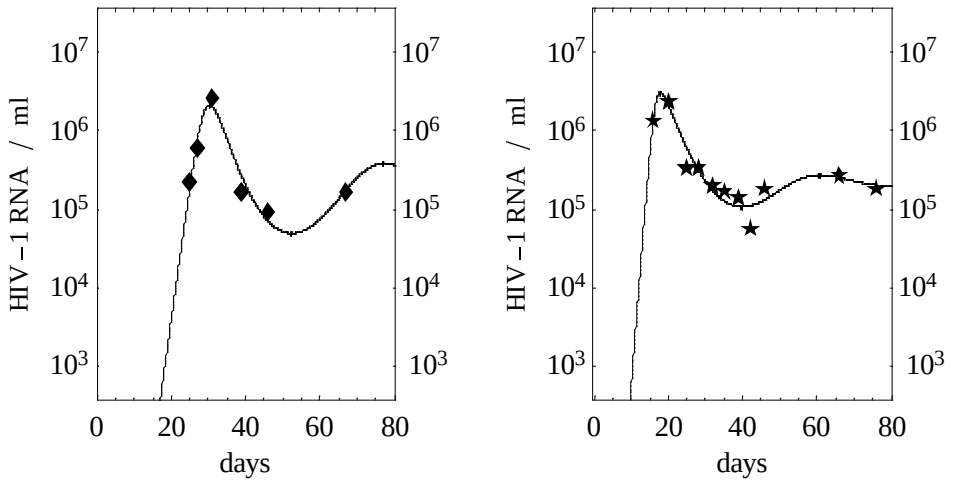

Figure 3. Theoretical curve using estimated parameters versus observed viral load data for patients 5 (◆) and 7 (⋆).

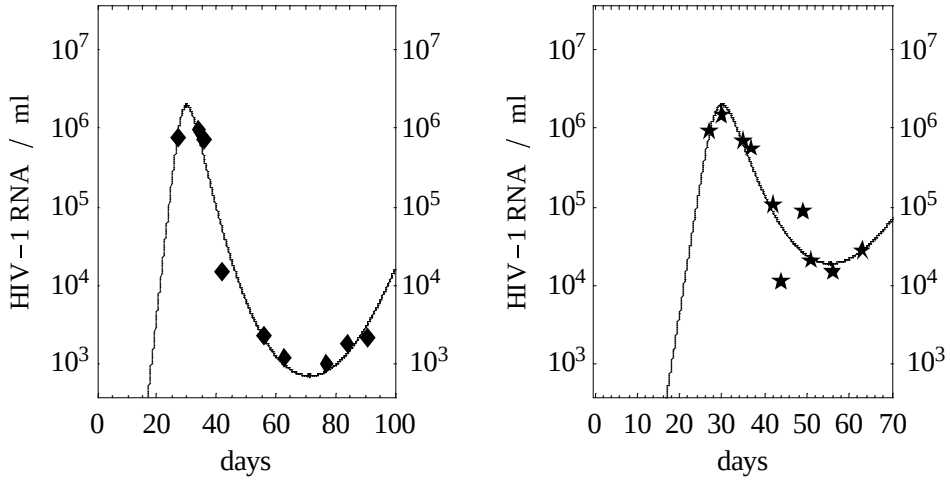

Figure 4. Theoretical curve using estimated parameters versus observed viral load data for patients 3 (◆) and 6 (⋆).

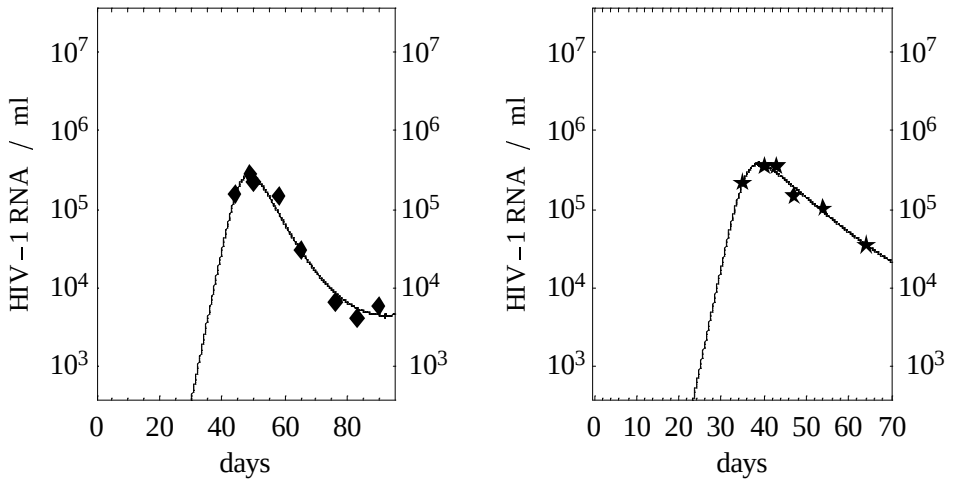

Figure 5. Theoretical curve using estimated parameters versus observed viral load data for patients 4 (◆) and 9 (⋆).

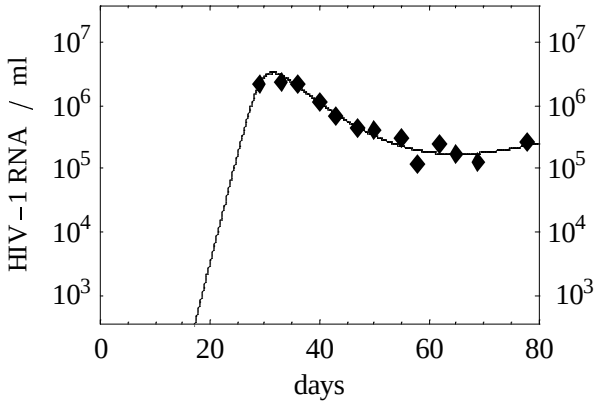

Figure 6. Theoretical curve using estimated parameters versus observed viral load data for patient 8 (◆).

There were too few points available for patients 1 and 2 to estimate all five parameters as above. By assuming time translation values similar to patients 3 through 9, however, it was not difficult to determine values for d, k, δ, and π that match the data. Simulation results and associated parameter estimates are provided in Fig. 7.

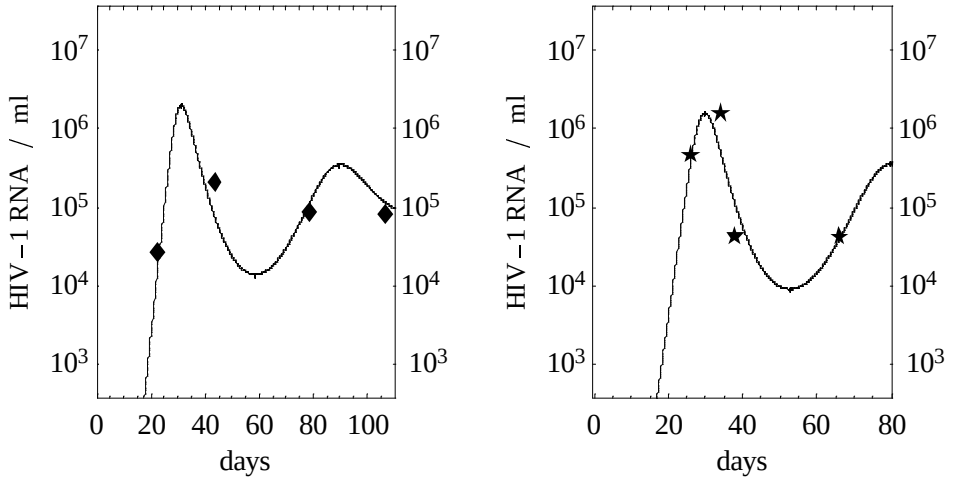

Figure 7. Theoretical curve using estimated parameters versus observed viral load data for patients 1 (◆) and 2 (★). Insufficient data points are available to estimate the time shift by the same method as for patients 3 through 9. Using similar times to peak as for the other patients, we determined the parameters by minimizing the objective function and found d, k, δ, and π to be [.0158, .000454, .5, 1052] and [0.0223, 0.00047, 0.812, 1285] for patients 1 and 2, respectively.

The steady state solution (T_{ss}, T_{ss}^*, and V_{ss}), reproductive ratio (R_0), and doubling time (T_2) are listed in Table 4. Eigenvalues of the approximate linear system, linearized about the steady state solution, were found to have negative real parts (results not shown) assuring a unique, asymptotically stable fixed point. The formulas used to compute R_0 and T_2 are taken from Bonhoeffer *et al*. (1997).

$$T_{ss}^* = \frac{\lambda}{\delta} - \frac{dc}{k\pi} \qquad V_{ss} = \frac{\pi\lambda}{\delta c} - \frac{d}{k} \qquad R_0 = \frac{k\pi\lambda}{cd\delta} \qquad T_2 = \frac{\ln 2}{\delta(R_0 - 1)}$$

Patient	T_{ss}^* (cells/μl)	V_{ss} (RNA/ml)×10^{-3}	R_0	T_2 (days)
3	0.244	86.1	3.24	0.605
4	0.573	25.6	3.2	1.22
5	0.637	222.	3.38	0.615
6	0.473	166.	3.28	0.607
7	0.77	215.	7.95	0.322
8	1.	310.	6.55	0.658
9	0.552	18.6	7.04	0.94
Mean	0.61	149	4.9	0.71
Sample SD	0.24	110	2.1	0.29

Table 4. Estimated steady state values of productively infected cell density (T_{ss}^*), viral load (V_{ss}), reproductive ratio (R_0), and doubling time (T_2) for patients 3 through 9.

4. Immune Responses

We shall show that when patient data is examined over periods longer than 100 days or so after infection, the target cell limited model fails to explain the data in many patients, with the viral load falling below the prediction. However, by including immune response mechanisms the data can be explained**.**

4.1 Longer Term Predictions versus Data

Figure 8 shows that patient 1's viral load following the peak declines to a value that is approximately 30% of the steady state value predicted based on only the first four data point. A steady upward trend ensues, with the final data point at day 267 nearly at the predicted steady state value

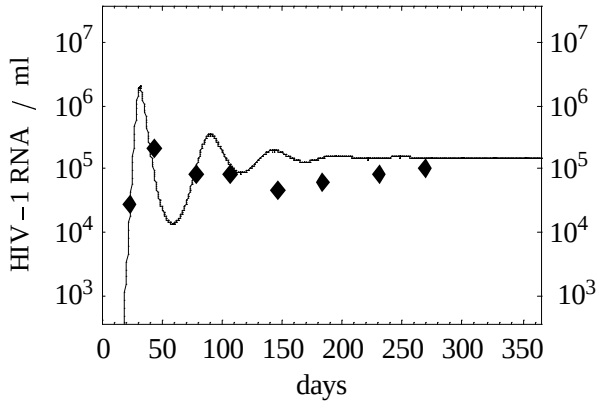

Figure 8. Theoretical curve generated using patient 1's best-fit parameters estimated using data from the first 100 days. Viral loads after day 140, which were not used in the parameter estimation, are below the theoretical curve increase steadily towards the predicted steady state value.

Patient 2's HIV-1 RNA concentration (Fig. 9) drops after the peak viremia to less than 10% of the steady state value predicted using the first four data points. By one year the viral load has nearly returned to the predicted steady state level. Nonlinear least squares estimation failed to converge when using the seven data points up to day 160, indicating that the simple model is not adequate to capture the processes occurring after the peak for this patient.

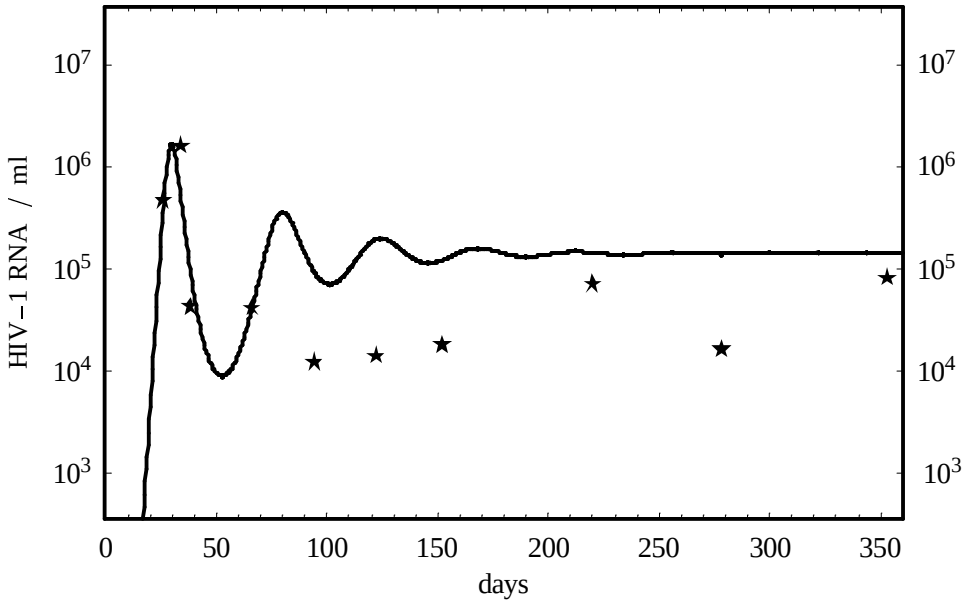

Figure 9. Predicted viral load changes for patient 2. Points after day 90, which were not used in the parameter estimation, show a decline well below the theoretical curve followed by an increase towards the predicted steady state value.

Patient 5's viral load drops only slightly below the predicted steady state level (Fig. 10). There are no data available for patient 7 between days 100 and 200, but we see that the predicted level is close to being attained by day 229.

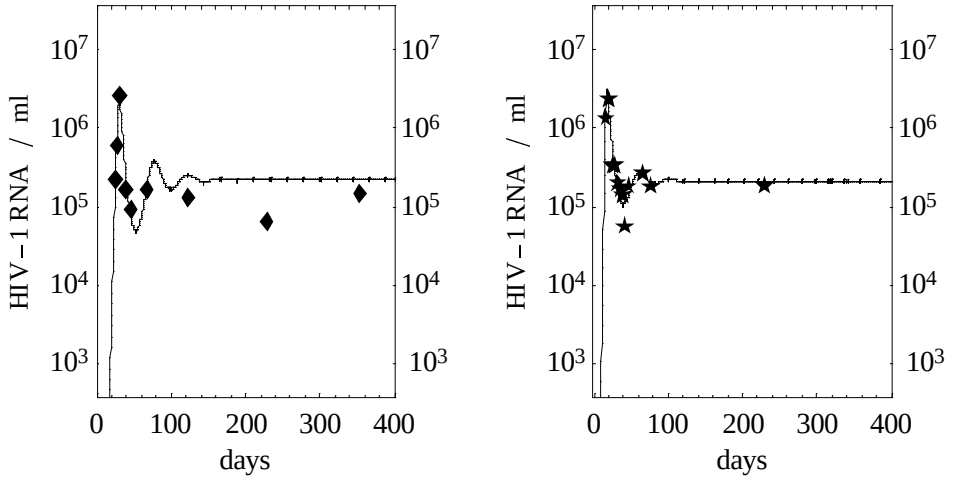

Figure 10. Theoretical curves generated using patient 5 (◆) and patient 7 (⋆) best fit parameters. Patient 5 data points after day 100, which were not used in the parameter estimation, show a slight decline below the theoretical curve while patient 7 data closely follows the prediction.

After the peak in viremia, the viral load of patient 6 (Fig. 11) falls well below the predicted steady state level and remains below. Again, the model does not adequately explain viral load declines of this magnitude.

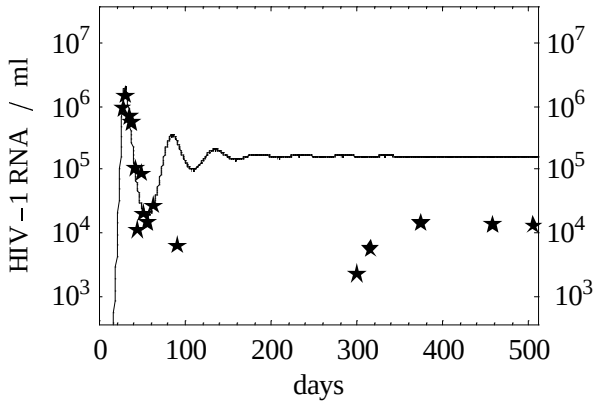

Figure 11. Theoretical curve generated using patient 6 best-fit parameters. Patient 6 data points after day 80, which were not used in the parameter estimation, are all well below the model's prediction.

Although patient data through day 100 was used for most patient data sets, patient 8 data after day 80 was not used. The reason for this exclusion is seen in Fig. 12 where the data points between days 85 and 104 fall below the predicted steady state value.

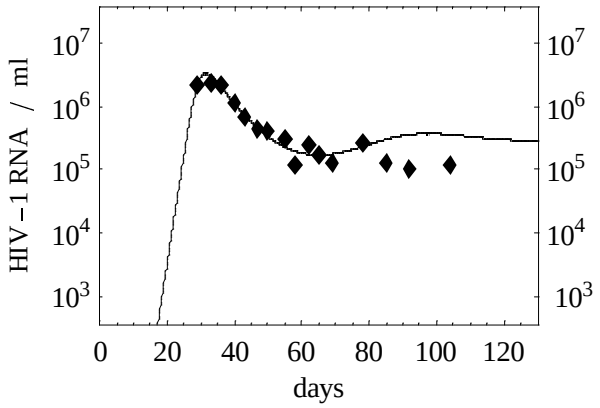

Figure 12. Theoretical curve generated using patient 8 best fit parameters. Patient 8 data points after day 80, which were not used in the parameter estimation, are significantly below the model's prediction.

Patient 9 (Fig. 13) is the only exception to the general trend. The final four points displayed were not used in the parameter estimation, and although the first two data points agree with the simulation, the final two points are well above the predicted steady state value. The model is not adequate in this case in that it does not predict an increase in viral load during this time interval, but it is consistent with the data through day 150.

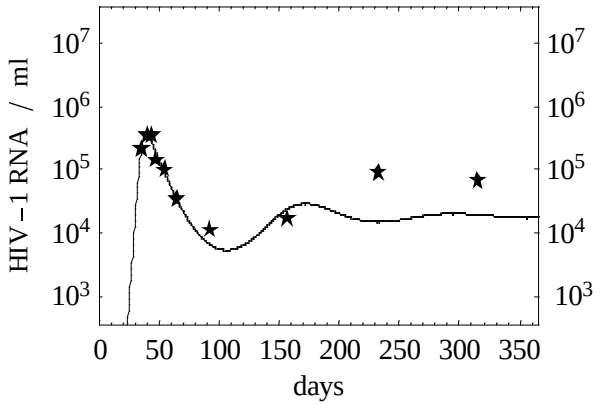

Figure 13. Theoretical curve generated using patient 9 best fit parameters. Two patient 9 data points after day 90 are significantly above the model's prediction.

In cases where viral load declines to very low values after the peak, as is the case for patients 3 and 6 (Fig. 4), the simple model predicts solutions that are highly oscillatory. Minimum viral loads following the peak for these two patients are approximately 1000 and 15,000 HIV-1 RNA copies/ml, respectively, compared with predicted steady state values of 86,000 and 166,000 HIV-1 RNA copies/ml. Insufficient data exists in these two cases to verify or refute the model's predictions of the one- to two-order increases in magnitude from the minima to the steady state levels, but such oscillatory behavior is not typically seen in data. Some additional HIV patient data (Fig. 14) show that viral load does not always rebound as our model would predict following steep declines. (Although there were no data points available to define the peak for these patients, parameter values similar to those in Table 3 were used to generate theoretical curves using our model.) The model's predictions clearly do not agree with patient data in the region just beyond the local minima at days 70 and 35, respectively.

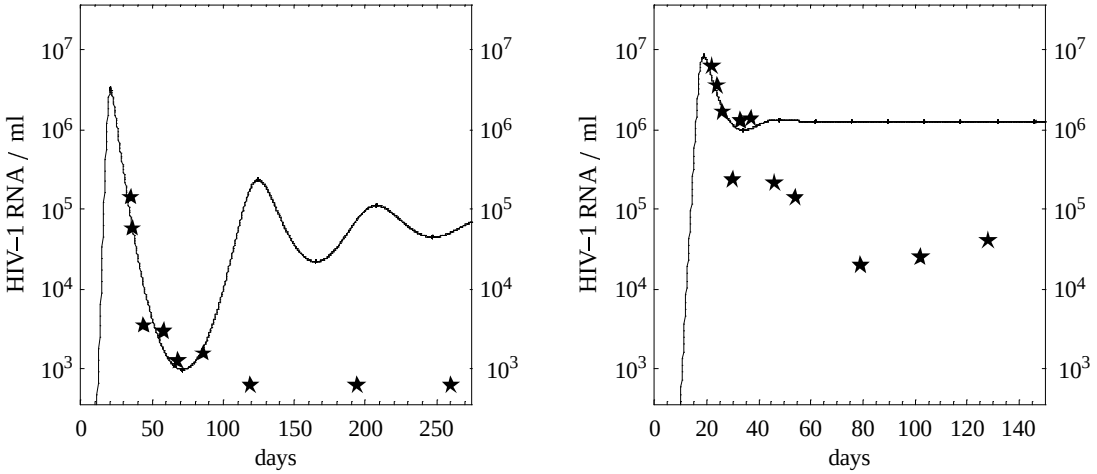

Figure 14. Theoretical curves using estimated parameters compared with two additional data sets from Aaron Diamond AIDS Research Center: MM (⋆) and VS (◆). Although no data exists for these patients near the peak, approximate values to mimic the rise and decline until the first local minimum in each case were determined. The target-cell limited model does not appear to be capable of matching these data sets.

On the other hand, viral loads of patients 1, 2, 5, and 7 do return approximately to the steady state values predicted by the model (Figs. 8 through 10). Additionally, Nowak *et al*. (1997a) report two cases of SIV-infected macaques whose SIV RNA levels increase more than an order of magnitude between 35 and 119 days post-infection. Comparing this data with patient 3 (Fig. 4), our patient exhibiting the most pronounced decline, we note that the model predicts a rise of less than two orders of magnitude from the lowest HIV concentration value.

In summary, using longer-term data we find significant deviations in viral load in some patients from the predictions of the target-cell limited model as early as 80 days following initial infection (patients 2 and 6). Patients 1, 5 and 8 showed slight reductions in the predicted viral loads, and patient 7 showed no deviation from predicted viral load (although there were no data points between day 80 and day 229). Only patient 9 had an increase above the predicted steady state value, the increase occurring more than 230 days following initial infection. Hence it is reasonable to speculate that some patients produce an immune response capable of reducing viral burden. To explore this possibility we modified our model to predict what might happen if there were either HIV-specific cytotoxic T lymphocyte (CTL) activity or suppression of HIV replication by cytokines such as (Maciaszek *et al*., 1997) or CAF (Mackewicz *et al*., 1995).

4.2 Models of Two Possible Immune Response Mechanisms

Typically immune responses are strongest when antigen levels are high. Here, rather than modeling the full CTL response, we simply assume that δ, the death rate constant of productively infected cells, increases due to CTL mediated cytolysis. The increase is assumed to be dependent upon the number of productively infected cells, which in turn is proportional to the virus concentration. Because the immune response takes time to develop, we assume that CTL activity is not substantial until after the peak viremia is reached. We make this assumption because several graphs of patient data seem to indicate that abrupt changes from the simple model's predictions occur most often as the viral load begins to climb for a second time. The form selected to model changes in δ with viral load is

$$\delta = \delta_0 + \delta(V) \quad \text{where} \quad \delta(V) = \begin{cases} 0 & t < t_V \\ f(t)V & t \geq t_V \end{cases}$$

The function *f(t)* is selected to allow the viral load-dependent expression to increase gradually over several days to mimic clonal expansion of a pool of effector cells. We selected the functional form

$$f(t) = \frac{\beta}{1 + \kappa e^{-\frac{(t - t_V)}{\Delta T}}},$$

but many other forms would give satisfactory results.

The simple model's prediction for patient 2's viral load does not match the data values beyond the first 75 days (Fig. 9). Incorporating a CTL response as described above, we find (Fig. 15) that the model can now mimic patient 2 data between days 90 and 160.

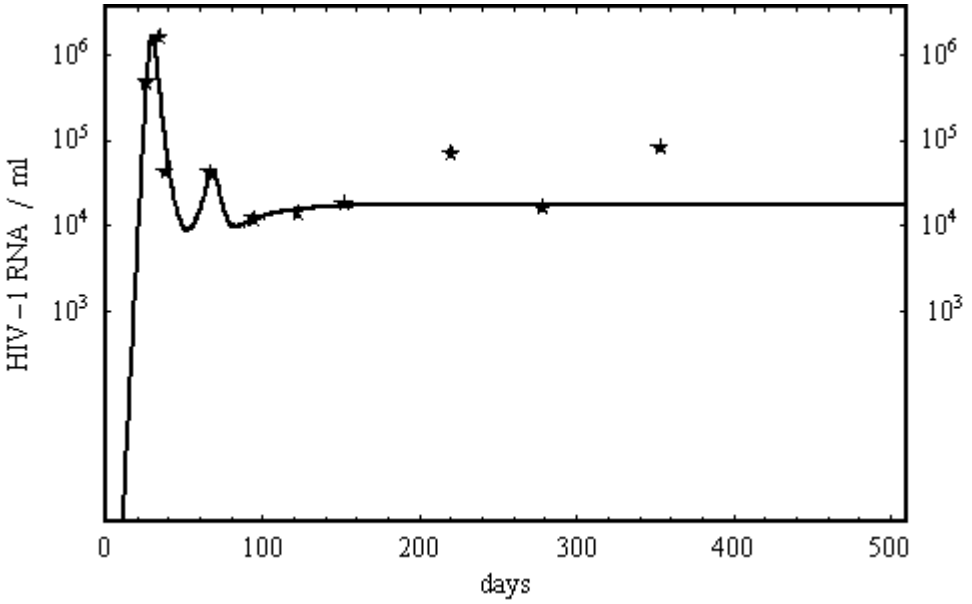

Figure 15. Theoretical curve for patient 2 with a CTL response initiated during the second rise in viral load.

The time history of the death rate parameter, δ, is shown in Fig. 16. An increase in δ to 1.4 day^{-1} is necessary to maintain a viral load of 1.76×10^4 HIV-1 RNA/ml. This value of δ is higher than values typically found from drug perturbation experiments (Klenerman *et al*., 1996). There are two data points nearer 10^5 HIV-1 RNA/ml. If we assume that these values reflect the patient's set point, then we find that a value of $\delta = 0.75$ day^{-1} is sufficient to maintain this steady state viral load (results not shown).

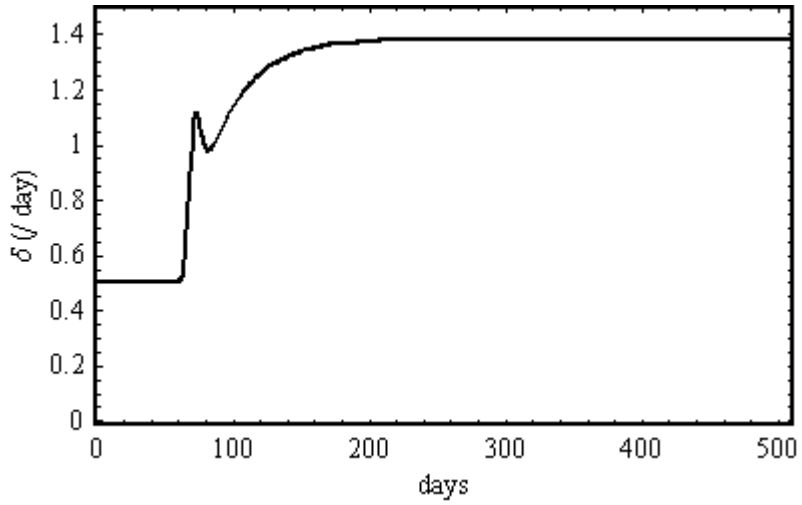

Figure 16. Inclusion of a CTL response requires the infected death rate constant, δ, to change over time as shown above. A final value of 1.4 day^{-1} is required to maintain the steady state viral load shown in Fig. 15. The temporal changes in the value of δ reflect changes in the viral load occurring after day 50.

Using the same functional form for δ, we obtained similar results for patient 6 (Fig. 17). Again, an unusually high final value of δ (1.4 day^{-1}) is needed to maintain the steady state value of approximately 10^4 HIV-1 RNA/ml. The change in δ over time (not shown) is nearly identical to the change needed for patient 2 (Fig. 16).

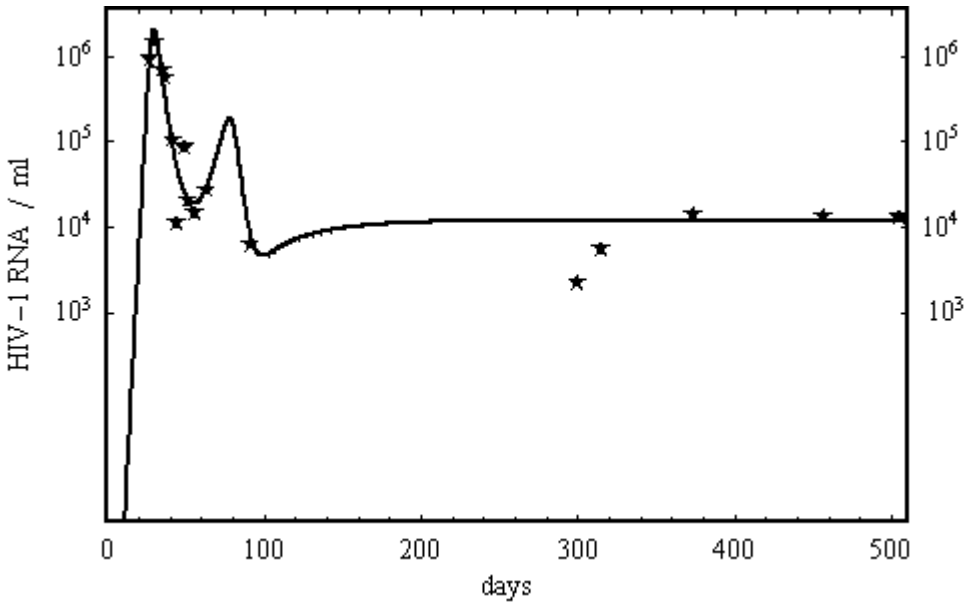

Figure 17. Theoretical curve for patient 6 with a CTL immune response function initiated during the second rise in viral load.

Another immune mechanism that has been suggested (Walker *et al*., 1986; Mackewicz *et al.*, 1995; Jin *et al*., 1999) is that a soluble factor produced by CD8+ T cells partially inhibits the production of virus particles by productively infected cells. The identity of this factor is unknown but Levy and coworkers have called it CAF, CD8+-cell antiviral factor (Mackewicz *et al*., 1995). We crudely simulated this form of response by reducing the virus production rate coefficient, π, to 35% of its original value at a time shortly following the first minimum in viral load. This yielded results for patient 6 that are strikingly similar to the data (Fig. 18). Interestingly, Jin *et al.* (1999) found that increasing π about three-fold gave reasonable agreement with viral load increases observed in SIV infected macaques after they were CD8+ T cell depleted.

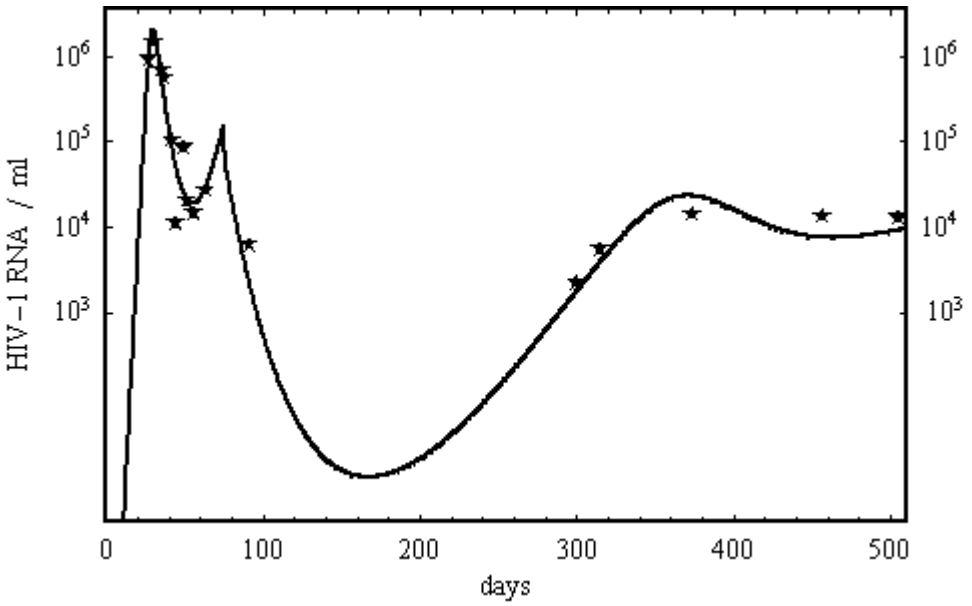

Figure 18. Theoretical curve for patient 6 incorporating a crude model of cytokine suppression. The production rate coefficient, π, was reduced to 35% of its value at day 70. If the change in π were made gradually then the sharp peak at day 70 could be converted into a more gradual change.

5. CD4+ T Cell Kinetics during Primary Infection

During primary infection not only does the viral load change but also the level of CD4+ T cell density changes. In this section, we use estimates obtained for parameters in the simplified model to make qualitative predictions of total CD4+ T cell density. To do this we use the full infected cell model (Eq. 2.2). Our simulations will also serve to partially legitimize the various assumptions made in deriving the simplified model.

Unfortunately, CD4+ T cell data is only available for three of the nine patients and of these data sets one is atypical and the other is over too short a time interval to be useful.

Hence, we only compare model simulation with one patient, patient 1. No baseline data exists on this or any of the other patients, but it is known that baseline total CD4+ T cell density varies widely across individuals. Sachsenberg *et al*. (1998) report a mean of 846 CD4+ T cells/microliter with a standard deviation of 230 cells/microliter for a group of 23 HIV-free control subjects (Sachsenberg *et al*., 1998). We found that a baseline value of CD4+ T cell density for patient 1 selected at the lower end of this range (650 cells/μl) gave a good fit with data.

A 900-day simulation (Fig. 19) of total CD4+ T cell density was conducted using the T cell kinetic model (Eq. 2.2) with parameter values depicted in Table 5. Note that the same values for parameters λ, k, δ, π, and c as determined in Section 3 are used. The value of d, the net loss rate constant in the simplified model, was used to determine the value of a, the rate constant for activation of quiescent cells. The only other differences in parameters from the uninfected model (Eq. 2.1) are due to enforcing equilibrium conditions at CD4+ T cell baseline of 650 cells/microliter

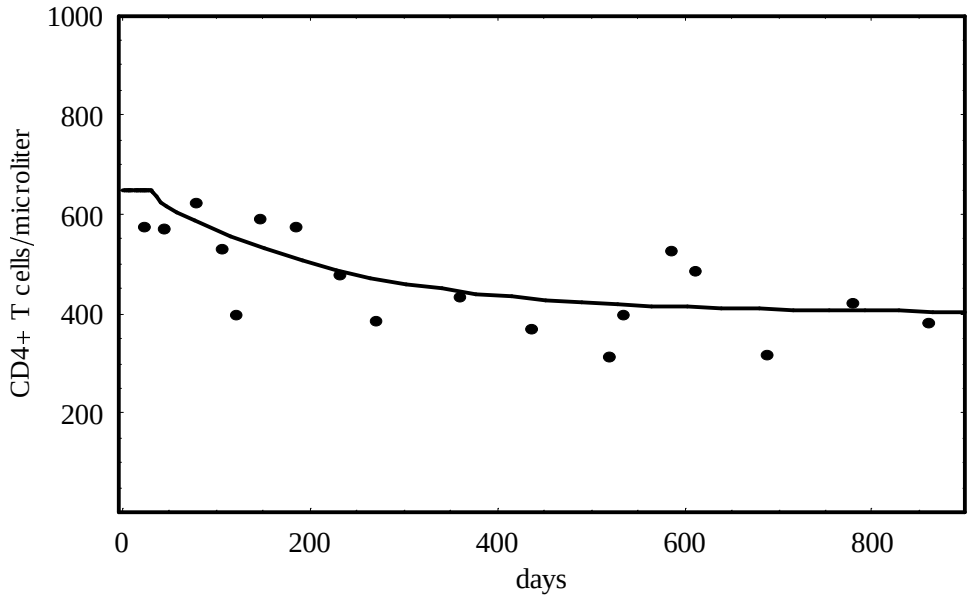

Figure 19. CD4+ T cell data from patient 1 (•) compared with simulation results using the full infected model (Eq. 2.2) with baseline density of 650 cells/μl.

Simulated versus observed viral load data over the 900 day simulation is also provided for comparison (Fig. 20). Model predictions of the various subsets of CD4+ T cell densities are shown in Fig. 21 although no patient data are available to validate the correctness of these predictions. We note, however, that for times greater than 100 days the number of activated producers of virus is essentially constant at the relatively low density of 0.14 cells/μl or about 0.7×10^6 cells in 5 liters of blood. Assuming 2% of infected cells are in blood, this yields a total body burden of 3.5×10^7 productively infected cells. Using the infected, activated cell death rate constant δ = 0.5 day^{-1}, we

estimate a turnover rate of infected cells of approximately 1.75×10^7 cells/day, which is similar to the estimate of 2×10^7 cells/day obtained by Haase *et al*. (1996) and about four-fold lower than the estimate given by Cavert *et al*. (1997) of 7×10^7 cells/day for patients in more advanced stages of disease.

Parameter	*Description*	*pt 1*	*Units*
P_{nom}	nominal precursor density	100	
Q_{nom}	nominal quiescent density	640	cells/μl
T_{nom}	nominal activated density	10	cells/μl
s	bone marrow source rate	.004	d^{-1}
r	Max growth rate of precursors	.05	d^{-1}
$\tilde{b}$	export rate of precursors	.015	d^{-1}
P_{max}	max precursor population	142.7	
T_{max}	max CD4+ T cell density	1500	cells/μl
μ_Q	death rate, resting cells	0.005	d^{-1}
μ_T	death rate, activated cells	0.2	d^{-1}
f	Fraction returning to quiescent cells	0.25	
a	activation rate constant	0.0004	d^{-1}
p	proliferation rate constant	0.37	d^{-1}
ϕ	relaxation fraction	0.05	
a_L	Latently infected cell activation rate	0.0004	d^{-1}
μ_L	Latently infected cell death rate	0.05	d^{-1}
δ	infected cell loss rate	0.5	d^{-1}
k	Activated cell infection rate constant	0.00045	$\mu l\ d^{-1}\ vir^{-1}$
π	Virion production rate constant	1050	$vir\ \mu l^{-1}\ d^{-1}$
c	virion clearance rate	3	d^{-1}

Table 5. Parameter values used for patient 1 in the full T cell kinetic model.

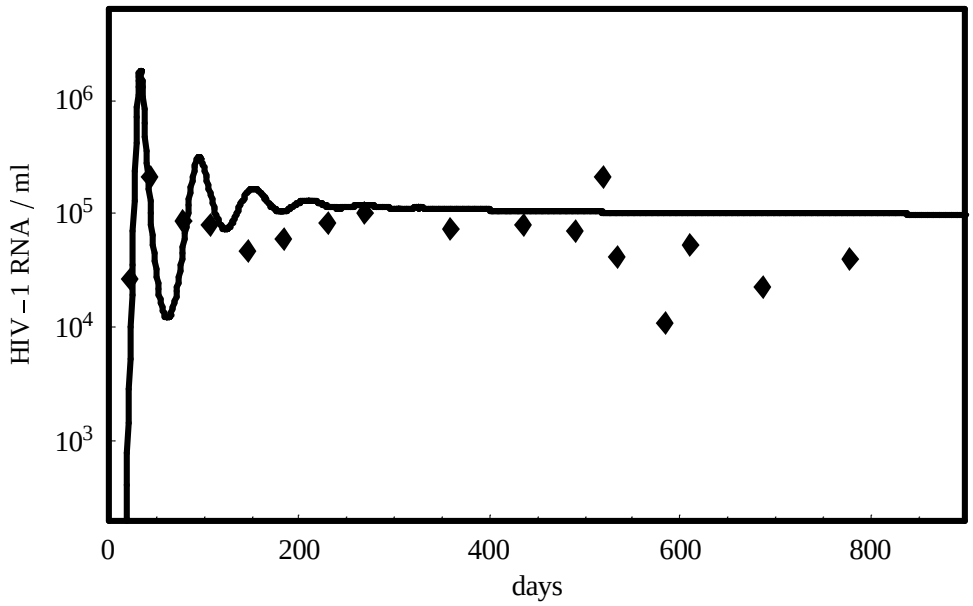

Figure 20. Viral load data from patient 1 (◆) compared with simulation results using the full infected model (Eq. 2.2) with baseline density of 650 cells/μl. (Although data is shown over 900 days, parameters d, k, δ, and π were estimated from only the first six data points.)

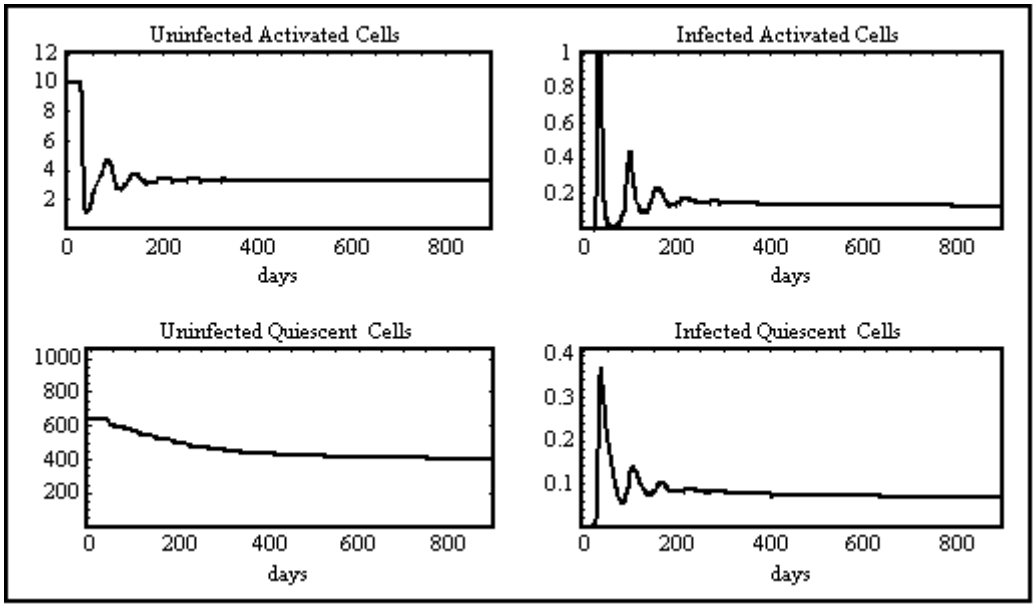

Figure 21. CD4+ T cell subsets from simulation using the full infected model (Eq. 2.2) with baseline density of 650 cells/μl. Values on all vertical axes are expressed in cells/μl.

As in the case for patient 1, the full model predictions of viral load during the first 100 days for all patients are nearly identical with the simplified model simulations (results not

shown) thus validating the assumptions made in using the simplified model for estimating parameters associated with viral dynamics.

Our model does not successfully mimic the observed data for all patients, however. For example, patient 9 CD4+ T cell data (Borrow *et al*. 1997) shows that this patient was a rapid progressor whose CD4+ T cell count was only 89 cells/microliter one year after initial infection. Neither our simplified model nor the full model produced results consistent with patient 9 CD4+ T cell data or viral load data after the first 100 days.

6. DISCUSSION

Although many complex processes occur during the rise and fall in viral load following initial HIV infection, we have shown that temporal changes in virus concentration observed early after infection are consistent with the assumptions embodied in the simplified target-cell limited model (Eq. 2.3). Relatively small variations in parameters determined by the host (d) and parameters determined by interaction between host and virus (k, δ, and π) can be used to account for the highly diverse patient-to-patient viral concentration transients observed during the first 100 days following primary infection.

We found a mean value of 0.34 day^{-1} for δ over patients 3 through 9, which is slightly less than the mean value of 0.37 day^{-1} determined by Klenerman *et al.* (1996) using data from five different drug perturbation experiments. In a separate study, a mean of 0.38 day^{-1} for δ was observed in primary infection patients given combination therapy a few days following onset of symptoms (Little *et al*., 1999). The very low values obtained for patients 8 and 9 (0.19 day^{-1} and 0.12 day^{-1}, respectively) may have skewed our results, particularly the data from patient 9, who progressed to AIDS in less than two years. The possibility that low values of δ, *i.e*., longer-lived productively infected cells, characterize patients who progress to AIDS rapidly is intriguing and needs to be examined in other cases.

We are unable to validate our results for the other parameter estimates as no conclusive, independent estimates, other than for δ, have been published to date. Further, dependencies between π and T_0 and between π and c, as shown in Appendix 1, imply that our estimates of π, c and T_0 are not unique.

Our results support, but do not conclusively prove, that the initial decline in viral load is due to target-cell limitation, as suggested by Phillips (1996), rather than to a response by the immune system. The model, which can be viewed as a minimal extension of the two-equation model widely used to interpret drug perturbation experiments, is able to match the highly diverse initial viral load transients by minor modification of parameters. Our parameter estimate of δ, determined using primary infection data, is consistent with estimates obtained in numerous other studies using patients in widely varying stages of progression (Klenerman *et al.*, 1996).

Two main arguments are often given to support the hypothesis of immune system control during primary infection. First, there is evidence of a temporal correlation between an increase in the HIV-1 specific CTL and CTL precursor frequency and decline in viral load (Koup *et al.*, 1994). Second, Matano *et al*. (1998) used anti-human CD8+ monoclonal antibody to deplete CD8+ T cells in macaques, either a few days before or a few days after inoculation with simian immunodeficiency virus (SIV). Measurements of SIV concentration showed marked increases in peak viremia as compared to controls, suggesting that CD8+ T cells are responsible for controlling the viral load.

These studies do not provide direct evidence, however, that CTLs are causing the HIV-1 viral load to decline from its early peak level. It may well be that many cytotoxic cells are generated as viral load increases and then, as viral load declines, the antigenic stimulus diminishes and the CTLs also decline. Thus the temporal correlation of CTL and virus as well as the inverse correlation between viral load and CTL do not establish to what extent CTLs are controlling the virus or simply responding to changes in antigen load. Further, *in vitro* it has been shown that the HIV-1 protein *nef* causes down regulation of MHC class I molecules on HIV-infected cells making such cells poor targets for cytolytic killing (Collins *et al*., 1998). Thus, while CTLs have the potential to shorten the lives of productively infected cells, these cells may be poor targets and, due to viral cytopathic effects, may already have a short lifespan. Perhaps an even stronger argument is that CTL activity during primary infection varies widely among HIV-1 patients (Musey *et al*.,1998), yet all nine of our patients' viral loads decline significantly from their peak values. Thus, it is not clear to what extent the large frequencies of CTLs observed in some studies are responsible for effectively eliminating productively infected cells, and hence causing the large drop in viral load observed during the first 30 to 50 days following initial infection.

The observation that anti-CD8 antibodies cause an increase in plasma virus levels supports the notion of CD8+ T cells playing a role in the control of viremia, although this effect may be mediated by soluble factors rather than CTL action. However, the experiment by Matano *et al*. (1998) is not definitive, as there is a plausible alternative explanation of their observations. We note that administration of anti-CD8 antibody to control animals AH37 and T14 generates significant changes in CD4+ T cell levels as well as CD8+ T cell levels. In fact, these animals' CD4+ T cell levels decline to approximately 25% and 50% of their respective baseline values by seven days following anti-CD8 monoclonal antibody injection. Such a significant change in the CD4+ T cell population implies that the monoclonal antibody does not simply remove CD8+ T cells. Major changes in cytokine production and in the degree of activation of CD4+ T cells may well be occurring, which in turn could significantly alter the virus concentration. The target-cell limited model, in fact, predicts much higher peak levels in viremia if the number of activated cells present at the time of initial infection is increased. We speculate that the low levels of CD4+ T cells found in the periphery seven days after injection with anti-CD8 monoclonal antibody is the result of their activation and sequestration in lymph nodes. The anti-CD8 antibody might be inducing pro-

inflammatory cytokines that simultaneously constrict the efferent lymph node ducts and produce an increase in activated CD4+ T cells that are SIV-susceptible.

In another SIV experiment (Schmitz *et al*., 1999), additional evidence is presented that suggests CD8+ T cells control viral load immediately following the peak in some monkeys. Again, anti-CD8 monoclonal antibodies were used to deplete the CD8+ T cells. Here, viral loads were only reported from the peak onwards. Although all five control animals had approximately the same peak values in viral load as those whose CD8+ T cells had been depleted, those with depleted CD8+ T cells on average maintained higher viral loads in the 28 days following the peak. In this experiment, unlike results reported in Mantano *et al*. (1998), the presence of CD8+ T cells did not affect the magnitude of the peak viral load since both the controls and the CD8-depleted animals had similar peak values.

In summary, although CD8+ T cells may influence viral load, the effect seen by Schmitz *et al*. (1999) occurred after the peak. Our models of primary infection also suggest that if CD8+ T cells are playing a role in primary infection, their main effect is seen predominantly late in the response and may not be directly responsible for bringing the peak viremia down. More detailed models of CTL activity and of the possible functioning of soluble factors, such as CAF, will be needed to more precisely elucidate their role in primary infection

7. SUMMARY

We have examined two models of HIV kinetics. The first of these is a minimal extension of a two-equation model frequently used to interpret drug perturbation experiments. We found that this *de facto* target-cell limited model can mimic the highly diverse temporal changes in viral load of nine patients during the first 100 days or so of primary HIV-1 infection. These results are consistent with, and provide evidence for, target cell limitation being the principle cause of the initial decline in viral load following the initial viremia peak. Using a second model, which includes CD4+ T cell kinetics, we demonstrated that the model matches the CD4+ T cell decline observed in one patient during the first several months of progression, and also yields a reasonable value for the number of productively infected CD4+ T cells. We also found that the simplified model is consistent with this more comprehensive T cell kinetics model, providing justification for the use of the standard three-equation model of HIV kinetics.

The standard target-cell limited model accurately predicts viral load in some patients well beyond the initial transient, but in other patients the viral load falls far below the model's prediction. This suggests that one or more unmodeled processes that lower the quasi-steady state viral load are present in these patients. We have explored two such processes—cytotoxic T lymphocyte (CTL) destruction of infected cells and suppression

by CD8+ cell antiviral factor (CAF). We find that models that include either one of these effects can mimic patient data, but thus far we are unable to clearly identify one or the other as dominant. Partial evidence in favor of CAF over CTL was obtained, however, since unrealistically high values of the productively infected death rate constant were needed to match the data in the two patients we considered. In either event, target-cell limitation alone cannot account for the ultimate determination of quasi-steady state viral load in some patients.

Appendix 1

In Section 3.2 it was asserted that two pairs of parameters (T_0 and π, c and π) in the simplified model are dependent. We now make that statement precise.

Dependency of T_0 and π

Suppose the uninfected equilibrium requirement, $\lambda = dT_0$ is used to eliminate the source term, λ, in equation 2.3, and define the initial value problem IVP1 by

$$\begin{aligned} \frac{dT(t)}{dt} &= d(T_0 - T) - kTV \\ \frac{dT^*(t)}{dt} &= kTV - \delta T^* \\ \frac{dV(t)}{dt} &= \pi T^* - cV \end{aligned} \quad , \quad \begin{aligned} T(0) &= T_0 \\ T^*(0) &= T_0^* \\ V(0) &= V_0 \end{aligned} \qquad \text{(IVP1)}$$

Let $\phi(t) = \left[\phi_1(t) \quad \phi_2(t) \quad \phi_3(t)\right]^T$ be the unique solution on some interval of interest, $[0,t_f]$. Define a second initial value problem, IVP2, by

$$\begin{aligned} \frac{d\tilde{T}(t)}{dt} &= d(\tilde{T}_0 - \tilde{T}) - k\tilde{T}V \\ \frac{d\tilde{T}^*(t)}{dt} &= k\tilde{T}V - \delta \tilde{T}^* \\ \frac{dV(t)}{dt} &= \tilde{\pi}\tilde{T}^* - cV \end{aligned} \quad , \quad \begin{aligned} \tilde{T}(0) &= \tilde{T}_0 \\ \tilde{T}^*(0) &= \tilde{T}_0^* \\ V(0) &= V_0 \end{aligned} \qquad \text{(IVP2)}$$

If $\tilde{T}_0 = \sigma T_0$ and $\tilde{\pi} = \frac{1}{\sigma}\pi$, then IVP2 has solution $\tilde{\phi}(t) = \left[\sigma\phi_1(t) \quad \sigma\phi_2(t) \quad \phi_3(t)\right]^T$ on the interval $[0,t_f]$. The proof is immediate.

The consequence of this result is that either the nominal target cell density, T_0, or the virion production constant, π, can be sought in parameter estimation using measurements of viral load alone, but not both. If methods are devised to make independent measurements of either of these, then the other can be sought using parameter estimation schemes such as the one we use in Section 3 which uses only viral load data.

Dependency of c and π

When $c \gg \delta$, a "quasi-steady state" approximation is sometimes used (Nowak *et al*., 1997b) to reduce the system of three equations in the simplified model to two differential equations and one algebraic equation:

$$\frac{dT(t)}{dt} = d(T_0 - T) - \frac{k\pi}{c} TT^*$$

$$\frac{dT^*(t)}{dt} = \frac{k\pi}{c} TT^* - \delta T^*$$

$$\overline{V} \equiv \frac{\pi}{c} T^*$$

Numerically it has been verified that for the values of c and δ in Table 3 that this system of equations gives solutions which are nearly identical with the original system. We note that neither π nor c appear individually but always as a ratio. Hence, we cannot distinguish between these two quantities from viral load data alone.

Appendix 2

We determined approximate time translations for each patient by constructing curves of minimum objective function values, J, versus δ for different values of the time shift parameter, τ. As an illustration of this process, we now consider data for patient 5 and construct these J versus δ curves for four different translation times: 21, 25, 28, and 32 days. The optimal values of δ, and the optimizing values of the other parameters, change with these different time shifts. We find (Fig. A1) the value of δ which minimizes the objective function to be approximately 0.37 day^{-1} for a translation of τ=21 days, 0.47 day^{-1} for a translation of τ=25 days, 0.57 day^{-1} for a translation of τ=28 days, and 0.75 day^{-1} for a translation of τ=32 days. The objective function values are lowest when data is shifted by approximately 25 days, corresponding to δ=0.47 day^{-1}, however there is only a relative difference of 1.6% in the minimum values of J between the 25- and 28-day cases. Generally, only data points earlier than 100 days post-infection were used for the estimation process. Translation times for patients 3 through 8 were all determined in this manner, although in some cases the method did not allow a sharp estimate.

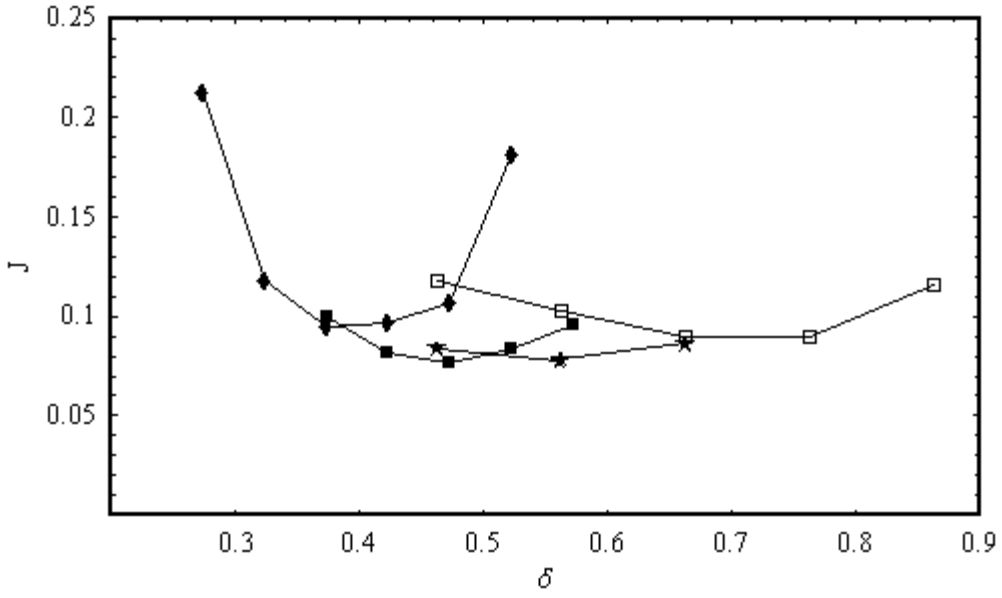

Figure A1. Translation times for patient 5 have strong affect on δ. Objective function values (J) versus infected cell death rate constant (δ) are plotted at several points of convergence of the least squares algorithm. Curves from left to right represent translation times of 21 (♦), 25 (■), 28 (⋆), and 32 (□) days. A translation of approximately 25 days for patient 5 corresponds to an optimal value of δ of approximately 0.47 day^{-1}.

To illustrate this point we show (Fig. A2) convergence points for varying translation times and different values of δ for patient 9. Although we know the translation time for this patient to be 35 days, there is essentially no variation in the minimum value of J as τ varies from 31 to 39 days. Clearly, this method would not have yielded a sharp estimate of τ. The minimizing value of δ, on the other hand, seems to consistently lie around 0.12 day^{-1} as the translation time varies between 31 and 39 days.

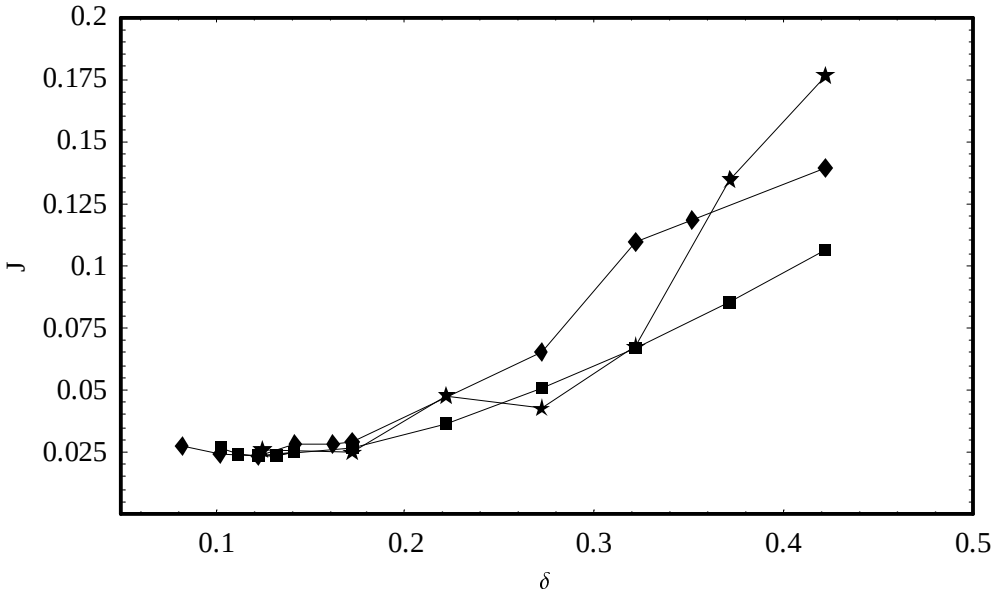

Figure A2. Translation times for patient 9 cannot be uniquely determined. Objective function values (J) versus infected cell death rate constant (δ) are plotted at several points of convergence of the least squares algorithm. The curves represent translation times of 31 (♦), 35 (■), and 39 (⋆) days.

Acknowledgments

Portions of this research were done under the auspices of the US Department of Energy. It was supported by faculty fellowships awarded to MAS by Associated Western Universities and the American Society of Engineering Education, Santa Fe Institute, as well as NIH grants RR06555 and AI40387, and a research grant from Texas A&M University-Corpus Christi. Data for Figure 2 were provided by Dr. Crystal Mackall, NIH. We also thank Eric Daar, University of Southern California and George Shaw, University of Alabama, for providing samples from their primary infection patients for analysis. The authors also wish to thank the patients who participated in the clinical trials.

Bibliography

ABBAS, A. K. (1996). Die and let live: eliminating dangerous lymphocytes. *Cell*, **84**, 655-657.

BONHOEFFER, S., MAY, R. M., SHAW, G. M., & NOWAK, M. A. (1997). Virus dynamics and drug therapy. *Proc. Natl. Acad. Sci. USA* **94**, 6971-6976.

BORROW, P., LEWICKI, H., WEI, X., HORWITZ, M. S., PEFFER, N., MEYERS, H., NELSON, J. A., GAIRIN, J. E., HAHN, B. H., OLDSTONE, M. B. A., & SHAW, G. M. (1997). Antiviral pressure exerted by HIV-1-specific cytotoxic T lymphocytes (CTLs) during primary infection demonstrated by rapid selection of CTL escape virus. *Nature Med.* **3**, 205-211.

CAVERT, W., NOTERMANS, D. W., STASKUS, K., WIETGREFE, S. W., ZUPANCIC, M., GEBHARD, K., HENRY, K., ZHANG, Z., MILLS, R., MCDADE, H., GOUDSMIT, J., DANNER, S. A. & HAASE, A. T. (1997). Kinetics of response in lymphoid tissues to anti-retroviral therapy of HIV-1 infection. *Science* **276**, 960-964.

CHUN, T., CARRUTY, L., FINZI, D., SHEN, ZUEFEI, S., DIGIUSEPPE, J. A., TAYLOR, H., HERMANKOVA, M., CHADWICK, K., MARGOLICK, J., QUINN, T. C., KUO, Y., BROOKMEYER, R., ZEIGER, M. A., BARDITCH-CROVO, P. & SILICIANO, R. F. (1997). Quantification of latent tissue reservoirs and total body viral load in HIV-1 infection. *Nature* **387**, 183-188.

CLARK, S. J., SAAG, M. S., DECKER, D. W., CAMPBELL-HILL, S., ROBERSON, J. L., VELDKAMP, P. J., KAPPES, J. C., HAHN, B., H. & SHAW, G. M. (1991). High titers of cytopathic virus in plasma of patients with symptomatic primary HIV-1 infection. *New Engl. J. Med.* **324**, 954-960.

COLLINS, K. L., CHEN, B. K., KALAMS, S. A., WALKER, B. D. & BALTIMORE, D. (1998). HIV-1 nef protein protects infected primary cells against killing by cytotoxic T lymphocytes. *Nature* **391**, 397-401.

DAAR, E.S., MOUDGIL, T., MEYER, R.D. & HO, D.D. (1991). Transient high levels of viremia in patients with primary human immunodeficiency virus type 1. *New Engl. J. Med.* **324**, 961-964.

ESSUNGER, P. & PERELSON, A. S. (1994). Modeling HIV infection of CD4+ T-cell subpopulations. *J. theor. Biol*. **170**, 367-391.

FAUCI, A. S. (1988). The human immunodeficiency virus: infectivity and mechanisms of pathogenesis. *Science* **239**, 617-622.

HAASE, A. T., HENRY, K., ZUPANCIC, M., SEDGEWICK, G., FAUST, R. A., MELROE, H., CAVERT, W., GEBHARD, K., STASKUS, K., ZHANG, Z.-Q., DAILEY, P. J., BALFOUR, H. H., JR., ERICE, A. & PERELSON, A. S. (1996). Quantitative image analysis of HIV-1 infection in lymphoid tissue. *Science* **274**, 985-989.

HRABA, T., DOLEZAL, J. & CELIKOVSKY, S. (1990). Model-based analysis of CD4+ lymphocyte dynamics in HIV infected individuals. *Immunobiol.* **181**, 108-118.

JIN, X. BAUER, D. E., TUTTLETON, S. E., LEWIN, S., GETTIE, A., BLANCHARD, J., IRWIN, C. E., SAFRIT, J. T., MITTLER, J., WEINBERGER, L., KOSTRIKIS, L., ZHANG, L., PERELSON, A. S. & HO, D. D. (1999). Dramatic rise in plasma viremia after CD8+ T-cell depletion in SIV-infected macaques. *J. Exp. Med.* (In Press).

KAHN, J. O. & WALKER, B. D. (1998). Acute human immunodeficiency virus type 1 infection. *New Engl. J. Med.* **339,** 33-39.

KIRSCHNER, D. E., MEHR, R. & PERELSON, A. S. (1998). Role of the thymus in pediatric HIV-1 infection. *J. AIDS* & *Human Retrovirol.* **18**, 95-109.

KLEIN, M.R., VAN BAALEN, C. A., HOLWERDA, A. M., KERKHOF GARDE, S. R., BENDE, R. J., KEET, I. P., EEFTINCK-SCHATTENKERK, J. K., OSTERHAUS, A. D., SCHUITEMAKER, H. & MIEDEMA, F. (1995). Kinetics of Gag-specific cytotoxic T lymphocyte responses during the clinical course of HIV-1 infection: a longitudinal analysis of rapid progressors and long-term asymptomatics. *J. Exp. Med.* **181**, 1365-1372.

KLENERMAN, P., PHILLIPS, R. E., RINALDO, C. R., WAHL, L. M., OGG, G., MAY, R. M., MCMICHAEL & NOWAK, M. A. (1996). Cytotoxic T lymphocytes and viral turnover in HIV type 1 infection. *Proc. Natl. Acad. Sci. USA* **93,** 15323-15328.

KOUP, R. A., SAFRIT, J. T., CAO, Y., ANDREWS, C. A., MCLEOD, G., BORKOWSKY, W., FARTHING, C. & HO, D. D. (1994). Temporal association of cellular immune responses with the initial control of viremia in primary human immunodeficiency virus type 1 syndrome. *J. Virol*. **68**, 4650-4655.

LINDSEY, J. W., HODGKINSON, S., MEHTA, R., SIEGEL, R. C., MITCHELL, D. H., LIM, M., PIERCY, C., TRAM, T., DORFMAN, L., ENZMANN, D. & STEINMANN, L. (1994). Phase 1 clinical trial of chimeric monoclonal anti-CD4 antibody in multiple sclerosis neurology. **44**, 413-419.

MCLEAN, A. R., SPINA, C. A., RICHMAN, D. D. & HAVLIR, D. V. (1999) Viral dynamics of acute HIV-1 infection. (submitted).

MACIASZEK, J. W., PARADA, N. A., CRUIKSHANK, W. W., CENTER, D. M., KORNFELD, H. & VIGLIANTI, G. A. (1997). IL-16 represses HIV-1 promoter activity. *J. Immunol*. **158**, 5-8.

MACKALL, C. L., FLEISHER, T. A., BROWN, M. R., ANDRICH, M. P., CHEN, C. C., FEUERSTEIN, I. M., HOROWITZ, M. E., MAGRATH, I. T., SHAD, A. T, STEINBERG, S. M., WEXLER, L. H. & GRESS, R. E. (1995). Age, thymopoiesis, and CD4+ T-lymphocyte regeneration after intensive chemotherapy. *New Engl. J. Med.* **332,** 143-149.

MACKEWICZ, C. E., BLACKBOURN, D. J. & LEVY, J. A. (1995). CD8+ T cells suppress human immunodeficiency virus replication by inhibiting viral transcription. *Proc. Natl. Acad. Sci. USA* **92,** 2308-231.

MATANO, T., SHIBATA, R., SIEMON, C., CONNORS, M., LANE, H. C. & MARTIN, M. A. (1998). Administration of an anti-CD8 monoclonal antibody interferes with the clearance of chimeric simian/human immunodeficiency virus during primary infections of rhesus macaques. *J. Viro*l., **72**, 164-169.

MCLEAN, A. R. & KIRKWOOD, T. B. L. (1990). A model of human immunodeficiency virus infection in T helper cell clones. *J. theor. Biol.* **147**, 177-203.

MCLEAN, A. R. & NOWAK, M. A. (1992). Models of interactions between HIV and other pathogens. *J. theor. Biol.* **155**, 69-102.

MITTLER, J. E., MARKOWITZ, M., HO, D. D. & PERELSON, A. S. (1998). Refined estimates for HIV-1 clearance rate and intracellular delay. (submitted).

MOHRI, H., BONHOEFFER, S., MONARD, S., PERELSON, A. S. & HO, D. D. (1998). Rapid turnover of T lymphocytes in SIV-infected rhesus macaques. *Science* **279**, 1223-1227.

MURRAY, J. M., KAUFMANN, G., KELLEHER, A. D. & COOPER, D. A. (1998). A model of primary HIV-1 infection. *Math. Biosciences* **154**, 57-85.

MUSEY, L., HUGHES, J., SCHACKER, T., SHEA, T., COREY, L. & MCELRATH, M. J. (1998). Cytotoxic-T-cell responses, viral load, and disease progression in early human immunodeficiency virus type I infection. *New Engl. J. Med.* **337,** 1267-1274.

NOWAK, M. A., MAY, R. M. & ANDERSON, R. M. (1990) The evolutionary dynamics of HIV-1 quasispecies and the development of immunodeficiency disease. *AIDS* **4**, 1095-1103.

NOWAK, M. A., ANDERSON, R. M., MCLEAN A. R., WOLFS T. F., GOUDSMIT, J. & MAY, R. M. (1991) Antigenic diversity thresholds and the development of AIDS. *Science* **254**, 963-969.

NOWAK, M. A., LLOYD, A. L., VASQUEZ, G. M., WILTROUT, T. A., WAHL, L. M., BISCHOFBERGER, N., WILLIAMS, J., KINTER, A., FAUCI, A. S., HIRSCH, V. M. & LIFSON, J. D. (1997a). Viral dynamics in primary viremia and anti-retroviral therapy in simian immunodeficiency virus infection. *J. Viro*l., **71**, 7518-7525.

NOWAK, M. A., BONHOEFFER, S., SHAW, G. M. & MAY, R. M. (1997b). Anti-viral drug treatment: dynamics of resistance in free virus and infected cell populations. *J. theor. Biol*. **184**, 203-217.

OGG, G. S., JIN, X., BONHOEFFER, S., DUNBAR, P. R., NOWAK, M. A., MONARD, S., SEGAL, J. P., CAO, Y., ROWLAND-JONES, S. L., CERUNDOLO, V., HURLEY, A., MARKOWITZ, M., NIXON, D.F. & MCMICHAEL, A. J. (1998). Quantitation of HIV-1-specific cytotoxic T lymphocytes and plasma load of viral RNA. *Science* **279**, 2103-2106.

PANTALEO, G., DEMAREST, J. F., SCHACKER, T., VACCAREZZA, M., COHEN, O. J., DAUCHER, M., GRAZIOSI, C., SCHNITTMAN, S. S., QUINN, T. C., SHAW, G. M., PERRIN, L., TAMBUSSI, G., LAZZARIN, A., SEKALY, R. P., SOUDEYNS, H., COREY, L. & FAUCI, A. S. (1997). The qualitative nature of the primary immune response to HIV infection is a prognosticator of disease progression independent of the initial level of plasma viremia. *Proc. Natl .Acad. Sci. USA* **94**, 254-258.

PAUL, W. E. (1993). *Fundamental Immunology, 3d ed*., New York, NY: Raven Press, Ltd.

PERELSON, A. S., KIRSCHNER, D. E. & DE BOER, R. (1993). Dynamics of HIV infection of CD4+ T cells. *Math. Biosciences* **114**, 81-125.

PERELSON, A.S., NEUMANN, A. U., MARKOWITZ, M., LEONARD, J. M. & HO, D. D. (1996). HIV-1 dynamics in vivo: virion clearance rate, infected cell life-span, and viral generation time. *Science* **271**, 1582-1586.

PHILLIPS, A. N. (1996). Reduction of HIV concentration during acute infection: independence from a specific immune response. *Science* **271**, 497-499.

REIBNEGGER, G., FUCHS, D., HAUSEN, A., WERNER, E. R., WENER-FELMAYER, G., DIERICH, M. P. & WACHTER, H. (1989). Stability analysis of simple models for immune cells interacting with normal pathogens and immune system retroviruses. *Proc. Natl. Acad. Sci. USA*, **86** 3026-2030.

RINALDO, C., HUANG, X., FAN, Z. F., DING, M., BELTZ, L., LOGAR, A., PANICALI, D., MAZZARA, G., LIEBMANN, J., COTTRILL, M. & *GUPTA, P*. (1995). High levels of anti-human immunodeficiency virus type 1 (HIV-1) memory cytotoxic T-lymphocyte activity and low viral load are associated with lack of disease in HIV-1-infected long-term nonprogressors. *J. Viro*l. **69**, 5838-5842.

RIVIERE, Y., MCCHESNEY, M. B., PORROT, F., TANNEAU-SALVADORI, F., SANSONETTI, P., LOPEZ, O., PIALOUX, G., FEUILLIE, V., MOLLEREAU, M;., CHAMARET, S., *M*, TEKAIA, F. & MONTAGNIER, L. (1995). Gag-specific cytotoxic responses to HIV type 1 are associated with a decreased risk of progression to AIDS-related complex or AIDS. *Aids Res. Human Retroviruses*, **11**, 903-907.

SACHSENBERG, N., PERELSON, A. S., SABINE, Y., SCHOCKMEL, G. A., LEDUC, D., HIRSCHEL, B. & PERRIN, L. (1998). Turnover of CD4+ and CD8+ T Lymphocytes in HIV-1 infection as measured by Ki-67 antigen. *J. Exp. Med*. **187**, 1295-1303.

SCHACKER, T., COLLIER, A., HUGHES, J., SHEA, T. & COREY, L. (1996). Clinical and epidemiologic features of primary HIV infection. *Ann. Int. Med.* **125**, 257-264.

SCHENZLE, D. (1994). A model for AIDS pathogenesis, *Stats. in Med.* **13**, 2067-2079.

SCHMITZ, J. E., KURODA, M. J., SANTRA, S., SASSEVILLE, V. G., SIMON, M. A., LIFTON, M. A., RACZ, P., TENNER-RACZ, K., DALESANDRO, M., SCALLON, B. J., GHRAYEB, J., FORMAN, M. A., MONTEFIORI, D. C., RIEBER, E. P., LETVIN, N. L. & REIMANN, K. A. (1999). Control of viremia in simian immunodeficiency virus infection by CD8+ lymphocytes. *Science* **283**, 857-1586-860.

SCHNITTMAN, S. M., LANE, H. C., GREENHOUSE, J., JUSTEMENT, J. S., BASERLER, M. & FAUCI, A. S. (1990). Preferential infection of CD4+ memory T cells by human immunodeficiency virus type-1: Evidence for a role in the selective T-cell functional defects observed in infected individuals. *Proc. Natl. Acad. Sci. USA* **87**, 6058-6052.

STEVENSON, M., STANWICK, T. L., DEMPSEY, M. P. & LAMONICA, C. A. (1990). HIV-1 replication is controlled at the level of T cell activation and proviral integration. *EMBO J.* **9**, 1551-1560.

STILIANAKIS, N. I., BOUCHER, C. A. B., DE JONG, M. D., LEEUWEN, R. V., SCHUURMAN, R. & DE BOER, R. J. (1997). Clinical data sets of human immunodeficiency virus type 1 reverse transcriptase-resistant mutants explained by a mathematical model, *J. Virol*. **71**,161-168.

WALKER, C. M., MOODY, D. J., STITES, D. P. & LEVY, J. A. (1986). CD8+ lymphocytes can control HIV infection in vitro by suppressing virus replication. *Science* **234**, 1563-1566.

WEI, X., GHOSH, S. K., TAYLOR, M. E., JOHNSON, V. A., EMINI, E. A., DEUTSCH, P., LIFSON J. D., BONHOEFFER, S., NOWAK, M. A., HAHN, B. H., SAAG, M. S. & SHAW, G. (1995). Viral dynamics in human immunodeficiency virus type 1 infection. *Nature* **373**, 117-123.

ZACK, J., HAISLIP, A., KROGSTAD, P. & CHEN, I. (1992). Incompletely reverse-transcribed human immunodeficiency virus type 1 genomes in quiescent cells can function as intermediates in the retroviral life cycle. *J. Virol.* **66**, 1717-1725.